Modelling the Contributing Factors of Hypoxic Fractions in Human Solid Tumors

by

Yijia Fan

Graduate Program in Medical Physics
Duke Kunshan and Duke University

Date:________________________
Approved:

____
Gregory Palmer, Advisor

____
Mark Dewhirst

____
David Huang

Thesis submitted in partial fulfillment of
the requirements for the degree of Master of Science in the Department of
Medical Physics in the Graduate School
of Duke Kunshan and Duke University

2021

ABSTRACT

Modelling the Contributing Factors of Hypoxic Fractions in Human Solid Tumors

by

Yijia Fan

Graduate Program in Medical Physics
Duke Kunshan and Duke University

Date:_______________________
Approved:

____
Gregory Palmer, Advisor

____
Mark Dewhirst

____
David Huang

An abstract of a thesis submitted in partial
fulfillment of the requirements for the degree
of Master of Science in the Graduate Program of
Medical Physics in the Graduate School of
Duke Kunshan ang Duke University

2021

Abstract

Hypoxia is one of the primary causes of radioresistance in human solid tumors. There are a series of contributing factors such as blood-flow rate, oxygen consumption rate, arterial pO_2, and microvascular arrangement. In this study, blood-flow rate, oxygen consumption rate (OCR), and arterial pO_2 are simulated to analyze their effects on hypoxia. A Green's function method is applied in a densely vascularized tumor region to predict oxygen delivery. The results indicate that changes in OCR lead to greater changes in hypoxia. A 30% reduction in oxygen consumption rate leads to a 21% reduction in the hypoxic fraction. However, a 30% increase in blood-flow rate and arterial pO_2 results in a 6% and 13% reduction in hypoxic fraction respectively. A 20% reduction in oxygen consumption rate plus a 20% increase in arterial pO_2 causes a 40% decrease in hypoxic fraction. With increasing blood-flow rate and arterial pO_2, hypoxic fraction reaches a plateau. As a result, hypoxia is more sensitive to OCR. In the second phase of this work, modeling results were compared to experimental data indicating the effect of papaverine in modulating tumor hypoxia. Papaverine is an FDA (Food and Drug Administration)-approved drug that can effectively decrease oxygen consumption rate and thus potentially decrease hypoxic fraction (~14%) at 2 mg/kg. At 4mg/kg, the addition of papaverine did not lead to a decrease in hypoxic fraction. This result fits the hypothesis that the oxygen consumption rate may be balanced by the effects of

vasodilation which may induce more tumor shunting and poor perfusion. However, the results shown here are limited to few animals. A larger number of animals in each group, combined with other types of evidence such as perfusion staining is conducive to get a more accurate result and a better understanding of the underlying mechanism. Therefore, these experiments can be regarded as preliminary results and suggest opportunities for future experimental work.

Contents

List of Tables

List of Figures

Acknowledgements

I would like to acknowledge my advisor, Dr. Greg Palmer, for offering me a lot of suggestions and guidance. He always encourages me to do what I want and offers me help in time. The COVID-19 makes the thesis work harder than ever. Dr. Greg is always patient to help me tackle with the problems I encountered. I would also like to acknowledge Dr. Secomb, who offers the model and helps me a lot. He is patient all the time and elaborates a lot in emails. I want to thank Dr. Dewhirst for serving as one of my committee members. I also thank Professor James, he would bear in mind every student's advisor, he is so dedicated. I would also thank Dr. David Huang for serving as my committee member. Although he cannot come back to school, he often expresses his concern via email or WeChat. I would like to thank Ashlyn Grace Rickard. She teaches me how to run the model step by step. She helps me on the experiment and also my thesis. She is truly kind.

I would also thank my classmates and friends for being with me. At last, I would express my thanks to my parents for supporting everything.

1. Introduction

It has been over 100 years since hypoxia has been regarded as one of the primary causes of radio-resistance in human solid tumors. The hypoxic regions in tumor tissues are determined by a series of factors such as blood-flow rate, oxygen consumption rate, blood oxygen content, and microvessels arrangement. Because of the therapeutic and clinical relevance, a lot of studies have been developed to reduce the hypoxic fraction in human solid tumors.

Although there are many approaches to study and modify hypoxia, a universal method to evaluate the impact of hypoxia-modifying factors is still lacking. Here, I applied a theoretical simulation model, which is formulated by Dr. Timothy Secomb from the University of Arizona, for predicting the distribution of oxygen-content in a typical, tumor-microvessel network. The results shown in this paper can assess the effects of factors mentioned above on the hypoxic fraction in human solid tumors.

1.1 Characteristic of hypoxia

Hypoxia can be divided into two categories: chronic hypoxia and cycling (or acute) hypoxia. Chronic hypoxia is defined as a constant oxygen-partial pressure (pO_2) value of less than 10mmHg in a tumor region. It is broadly caused by a lack of effective and organized vasculature [3]. Cycling hypoxia is described by fluctuations in pO_2 values, which is the result of an imbalance between oxygen supply and demand [4].

Compared with normal tissues, hypoxic cells are less radiosensitive to radiation. In the early 1900s, Schwartz published the first paper suggesting that oxygen was negatively affecting radiotherapy. He stated that skin responded worse to radiation if the blood flow was decreased [1]. Then, Gray and his group also demonstrated in 1953 that hypoxia could be the influencing factor of radio-resistance in tumors [2].

It is well-established that hypoxia exists in most human solid tumors [23]. The reduced oxygen-content in microvessels result in poor response to radiation and harm other biological functions. Radiation is effective due to two mechanisms: direct interactions with tissue DNA which results in a double-strand DNA break and cell apoptosis, and indirect interactions in which radiation interacts with the tumor microenvironment to produce free radicals that cause single-strand DNA breaks, leading to cell death [65]. The latter interaction is not only more probable and represents most of the radiation-tumor interactions, but it also requires an abundance of free oxygen molecules to produce the free radicals [65]. The effect of hypoxia on chemotherapy efficacy is more straightforward: most chemotherapies are delivered intravenously; if the vasculature is leaky, disorganized, and heterogenous, the chemotherapy cannot perfuse all tumor regions [66].

In general, hypoxia has three characteristics: (i) complexity and heterogeneity across individuals [22], (ii) prevalence in almost human solid tumors [23], (iii) dependence on the pathophysiology of tumor vasculature. Due to these three characteristics, it is difficult to implement a single, effective method to treat hypoxia in clinical studies.

1.2 Causes of Hypoxia

In brief, the occurrence of hypoxia is caused by deficiencies between oxygen demand and supply. In addition, hypoxia is strongly influenced by the microvascular network. There are seven factors that can give rise to hypoxia: (i) Scant arteriolar supply. This takes place in the tumor region whose microvessels are too far from arterial sources to transport oxygen [36]. (ii) Sparse vascular distribution. When the distance between microvessels is larger than the oxygen diffusion distance in tumors, these regions are regarded as hypoxic regions [37]. (iii) Inefficacious microvascular distribution. The distribution of microvessels is highly related to tissue pO_2 values, the inefficacious vessel distribution can result in hypoxia in some tumor regions [38]. (iv) Flux fluctuations in red blood cells. If the flux in red blood cell varies rapidly or even no red blood cells exist in the tumor vasculature, on these occasions, hypoxia is likely to occur [39]. (v) Variations of hypoxic red blood cells. Once the red blood cells are hypoxic, they will experience a series of changes such as shrinkage, insensitiveness, flux decrease ,etc., which can lead to more severe hypoxia [24]. (vi) Existence of blood shunts. The transport of blood in vessels is stable. But the occurrence of blood shunts between arteries and veins will break this stability [40].

1.3 Effects of hypoxia on tumor cells

Dozens of studies have demonstrated that hypoxia is highly correlated with poor prognosis since lack of oxygen is conducive for tumors to overcome adverse surroundings [44]. Moreover, since hypoxia takes part in the full process of tumor proliferation, it lays the foundation for tumor metastasis [45].

Studies dating back more than 30 years have shown that hypoxic tissue was three times less radiosensitive than normoxic tissue [41]. In addition, hypoxia in tumor regions can result in discrepancies between IMRT plan and real tumor volume, which hinders the development of targeting hypoxic regions in human solid tumors [22]. On the other hand, if the red blood cells become hypoxic, the changes such as insensitiveness and shrinkage will inhibit vasculature to transfer nutrients to a tumor and thus be resistant to chemotherapy [43].

1.4 Hypoxia modifying therapies

The common purpose of all hypoxia modification therapies is to improve radiation response by reducing hypoxic fractions. Dewhirst concluded in 2018 that there were four approaches to achieve this goal: (i) increasing oxygen supply, (ii) reducing oxygen consumption rate, (iii) addition of radiosensitizing drugs, (iv) killing hypoxic cells selectively [5].

Increasing oxygen supply

The most obvious way to improve the imbalance between oxygen supply and demand would be to increase the oxygen supply. The initial experiment was conducted by Davidson in 1955, who was the first to prove that hyperbaric oxygen was beneficial to human tumors [6]. This result has attracted the attention of many scholars. Around 10 years later, one experimental study concluded that under hyperbaric conditions, both oxygen and hydrocarbon respiration can greatly meliorate the radiation response of tumors [7]. However, due to its discomfort to patients and high cost, hyperbaric oxygen combined with RT treatment cannot be performed routinely in the clinic. Nevertheless, studies in the 20th century have shown that hyperbaric oxygen can treat late radiation damage [8]. Under normobaric conditions, experiments have also been attempted to ameliorate radio-resistance caused by hypoxic fractions in solid tumors, but there was no significant improvement [9]. In 2018, Samantha et al. stated that lipid-stabilized oxygen microbubbles (OMBs) can increase tumor oxygen levels *in vitro* and *in vivo* for tens of minutes. Moreover, they found that a fixed microbubble dose before radiotherapy can control tumors effectively. Since large tumors are more likely hypoxic, the smaller tumor has better control than large tumors [67]. Over time, other methods that aim to increase oxygen supply include transfusion of red blood cells, artificial blood substitutes [23], erythropoiesis-stimulating agents, and microcirculatory-stimulating agents [24]. Additionally, it is accepted that changing the oxygen consumption rate is much more effective than changing the oxygen delivery [11].

Modifying oxygen consumption rate

Secomb concluded in 2009 that reducing oxygen consumption rate is more effective to decrease hypoxic fraction than modification of blood-flow rate and arterial pO_2 [61]. One of the efficacious methods to decrease oxygen consumption rate is the administration of papaverine. In 1848, Merck first isolated papaverine (PPV), which has multiple biological effects, from *papaver somniferum* [46]. It allows for widening of blood vessels, which results from the relaxation of smooth muscle cells within the vessel walls, in the large veins, large arteries, and smaller arterioles [55]. In the clinic, papaverine is used as a muscle relaxant and antispasmodic [55]. The reason for its vascular effects is that it has an inhibitory effect on mitochondrial complex I [57].

As a radiosensitizer, papaverine has been proven to decrease tumor-cell oxygen consumption rate significantly by inhibiting mitochondrial function, thus mitigating tumor hypoxia [57]. As shown in figure 1, in E0771 tumor cells, papaverine decreases OCR dramatically in the first 30-40 min in a dose-dependent manner. At 10 μM, papaverine decreases OCR nearly to half [57].

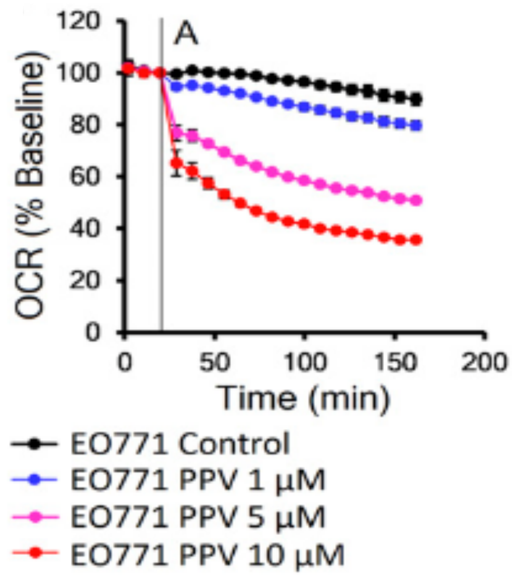

Figure 1: Papaverine effects in OCR in E0771 cells.

This figure indicates that papaverine reduces OCR in a dose-dependent manner in E0771 tumor model [57].

In terms of human solid tumors, previous studies showed positive effects on prostate tumors [49]. Hang Huang et al. demonstrated that papaverine can be selective and dose-dependent toxic to PC-3 cells and showed no negative effects on human normal tissue, whereas most existing antitumor drugs present toxicity in both tumor cells and normal human fibroblasts [54]. The author demonstrated that the antitumor effect was induced by mitochondrial-mediated apoptosis, cell cycle arrest, and downregulation of the NF-kB/PI3K/Akt pathway [54]. Such antitumor effects have been studied in other types of tumors such as melanoma [49], colorectal tumors [51], breast tumors [51], and hepatocarcinoma [53].

Addition of radiosensitizers

Another feasible and extensively studied approach to overcome hypoxic cells is to apply biochemical agents to radiosensitize hypoxic cells. It was found by Adams and co-workers that the mechanism of radiosensitization was associated with electron affinity [12]. One possible radiosensitizer was Metronidazole, which was first studied by Overgaard. He explored the potential of Metronidazole as a kind of radiosensitizer in clinical trials, but the experiment did not show any significant benefit [13]. Calais discovered that Clofibrate would restrain the binding of hemoglobin and oxygen and therefore serve as a possible radiosensitizer [14]. In the same year, Kiellen et al. found Nicotinamide can be a vasoactive agent, whose function was to prevent transient closure of blood vessels thus eliminating acute hypoxia [15]. Additionally, meta-iodobenzylguanadine (MIBG) was also verified to hinder oxygen consumption in solid tumors [16]. Pentoxifylline had the same function as MIBG but the mechanism of Pentoxifylline was to decrease blood glutinosity and vasodilation [17]. Such agents involve Efaproxiral found by Wahr in 2001. Efaproxiral has been proven to reduce the binding affinity between hemoglobin and oxygen thus increasing pO_2 values [18]. Overall, the observed radiosensitizers that have been tested in clinical trials have shown effectiveness only in the head and neck, and to a lower degree in bladder tumors. The exploration of less toxic and more effective radiosensitizer agents has to continue.

Killing hypoxic tumor cells

Reviewing previous studies, Coleman et al. demonstrated, “The derivatives of the classic 2-nitroimidazole compounds such as SR-2508, and bifunctional compounds, such as RSU-1069, can be toxic to hypoxic cells after prolonged incubation under hypoxia” [20]. The mechanism of this method is that these compounds can only be activated by bioreductive processes in hypoxic regions. However, the experiment had to be stopped due to the neurotoxicity in clinical trials. Subsequently, Zeman et al. found Non-nitro compound SR-4233, which was more effective to kill hypoxic tumor cells *in vitro* [21]. In addition to nitroimidazole derivatives, other agent such as Tirapazamine, whose function is to damage DNA helix in hypoxic regions, is also considered as a potential radiosensitizer. Early trials of Tirapazamine in head and neck tumors had shown promising results, but it led to muscle toxicity and ultimately failed [19]. These findings are vital to clinical research but cumbersome to carry out since the effectiveness of toxic agents highly depends on the exposure of the agents to cells while they are hypoxic. Therefore, this method is especially hard to implement in acute hypoxia conditions.

Dozens of papers have been published about reducing hypoxic fractions in tumor regions by approaches mentioned above. Recent research has placed focus on the combination of nanotechnology and medicine. There are four classifications of nanoparticle-mediated strategies: (i) improving the tumor microenvironment, (ii) increasing oxygen delivery to tumors, (iii) generation of oxygen, (iv) making use of hypoxia [31].

In terms of modifying tumor microenvironments, such conditions as temperature, hyaluronan, and tumor vasculature, are common manipulated to affect hypoxia [32-35]. Besides, many pathways are influenced by hypoxia, such as angiogenesis, glucose transport, PH regulation, and erythropoiesis [26]. One of the pathways worth mentioning is a transcription factor hypoxia-inducible factor-1 (HIF-1) which plays a vital role in modifying tumor radiosensitivity [25]. It is well-established that in more than 50% head and neck tumors, HIF-1 overexpression correlates with poor RT performance [27]. Suppression of HIF-1 activity will radiosensitize tumors [28]. The mechanism is likely because HIF-1 causes tumor cells to express radioprotective cytokines that act on neighboring endothelial cells [29]. For increasing oxygen content to tumor cells with nanoparticles, most emerging trials bind nanoparticles on red blood cells (RBC) inside the tumor, since RBCs usually take charge of delivery and release oxygen to assist therapy.

1.5 Research Objective

There are many factors such as microvascular arrangement, blood-flow rate, oxygen consumption rate, and arterial pO_2 content that can affect hypoxic regions in human solid tumors. In addition, applications of radiosensitizers - such as papaverine- are feasible approaches to overcome hypoxia in tumor. In this study, in a region whose microvascular geometry is derived from a transplanted mammary adenocarcinoma (R3230AC) in a rat dorsal skin flap preparation, the effects of OCR, blood-flow rate and arterial pO_2 are simulated theoretically. At the same time, the effectiveness of papaverine to reduce hypoxia is compared with the above mentioned factors.

2. Methods

This Green's function method contains three sections to modify hypoxia: vessel arrangement, oxygen-diffusion simulation, theoretical model simulation.

Vessel arrangement and model parameters

I used the microvessel configuration that Dr. Secomb used in 1995 [61]. Briefly, a window chamber was set on a dorsal skin flap of a Fischer-344 rat. A clear network of vessels was chosen one week after a piece of mammary adenocarcinoma (R3230AC) was introduced into the selected region (figure 2). The selected region was 0.25 mm × 0.37 mm × 0.2 mm, containing 22 segments observed in tumor tissue [62]. The network information such as location and flow directions were saved in television records [60]. From videotape, the magnified tissue microcirculation was constructed. To obtain the velocity of red blood cells, a dual-slit method was applied [60].

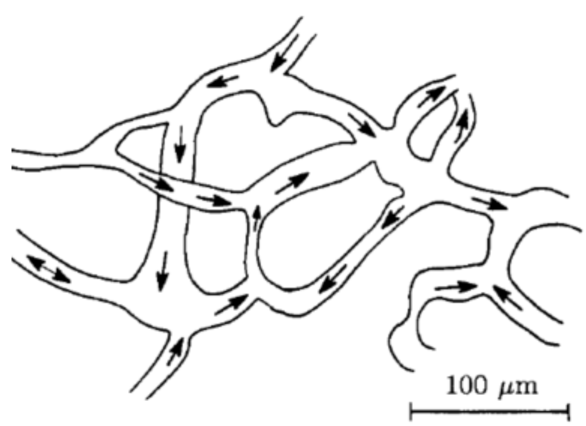

Figure 2: Tumor microcirculation at 130X magnification [62].

This network was obtained from a dorsal skin flap of a Fischer-344 rat which has been introduced with R3230AC. Tracing of microvessels in tumor was from video image.

Oxygen diffusion simulation.

The tumor microcirculation was simulated with a Green's function method [38]. This method measures the vessels and junction's location directly from the geometric maps, then divides each vessel into 100-200 small segments, and makes every section uniform and straight. The discretized configuration is shown in figure 3.

There are several assumptions in this method. (1) The selected tissue region is homogeneous, both oxygen diffusivity and solubility are uniform. (2) The vessels are assumed to be a series of finite cylindrical segments; Vessel walls are considered as parts of the tissue space. (3) In the selected field, a steady-state condition for input arterial pO_2 is supposed.

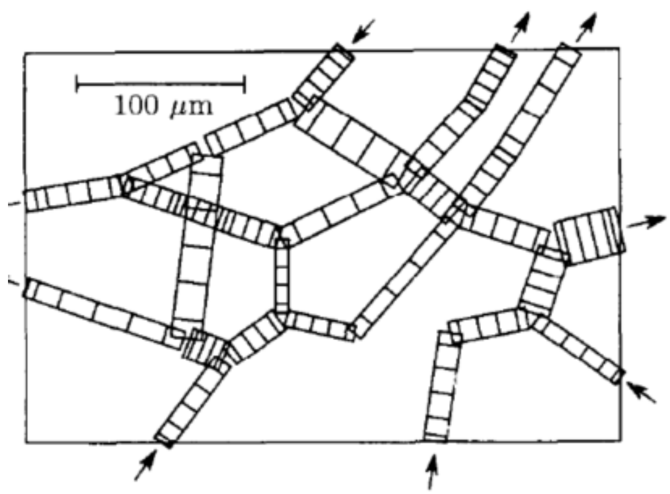

Figure 3: Simulated tumor microcirculation at 130X magnification [62].

The geometric map are discretized into 100-200 short segments. Each segment is uniform and straight.

In the selected tumor microcirculation network, a Green's model method is applied to predict and analyze the oxygen delivery. As shown in figure 4, the Green's model applies the Cartesian coordinate system (x_1, x_2, x_3).

In the discretized region, there are over 100 segments. For each segment, the oxygen consumption rate is supposed to relate to arterial pO_2 with the Michaelis-Menten relationship:

$$M(C) = M_0 \frac{C}{C+\alpha P_M} \quad \text{(Eq.1)}$$

where M_0 is the oxygen consumption rate (OCR), C is arterial pO_2, P_M is the pO_2 value when OCR reduces to half, α is the solubility. The selected field's oxygen condition is indicated by the rate of oxygen efflux.

Theoretical model simulation.

These segments' oxygen concentration is computed by an iterative method. Then, there is a linear relationship between oxygen concentration and source strength so that for each segment, vessel pO_2 can match with tissue pO_2 at the blood-tissue boundary. Finally, pO_2 can be computed at any point, then the hypoxic fraction can be estimated from computed pO_2 values at randomly selected points in the region.

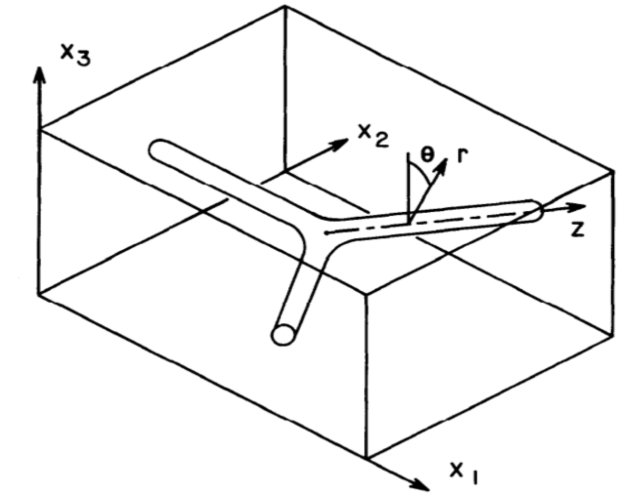

Figure 4: Cartesian system (x1, x2, x3) for selected tumor region [63].

The cylindrical polar system inside is for one vessel segment.

The oxygen content in the blood is obtained by equation (2), where P is arterial pO_2, P_{50} is 38 mmHg, n=3, α is solubility and equals 3.1×10^{-5} cm^3 O_2/cm^3/mmHg.

$$C = C_0 \frac{(P/P_{50})^n}{1+(P/P_{50})^n} + \alpha P \qquad \text{(Eq.2)}$$

In my computation, arterial pO_2 is 100 mmHg, both OCR and blood flow rate are modified from -50% to 50% based on default baseline values. There are three variables in our computation, OCR, arterial pO_2, and blood-flow rate. All these three variables are changed with respect to control values, i.e., OCR=$M_{control}\times M_{rel}$, pO_2=$P_{control}\times P_{rel}$, blood flow rate=$Q_{control}\times Q_{rel}$. The detailed parameter values are listed in table 1.

Table 1: Parameter values in simulation region

Parameter	
P_{50}	38 mmHg
n	3
Number of nodes	1200
OCR range	0.00025-0.00075 cm^3 O_2/g/s

	(relative to default value 0.0005)
Flow rate range	0.0868-0.2605 (multiplicative value, relative to default value 0.1736)
Arterial pO_2	100mmHg

Murine Tumor Models for In Vivo Imaging

Two murine models were used to quantify the changes in tissue oxygen due to papaverine. The E0771 tumor model used cells sourced from CH3; these were cultured in RPMI media supplemented with 10% v/v heat-inactivated fetal bovine serum and 1% v/v penicillin/streptomycin. E0771 cells were maintained in standard cell culture conditions: 5% CO_2 and 37°C. 200,000 E0771 cells were suspended in sterile PBS and injected subcutaneously into the flanks of 5, female C57Bl/6 mice sourced from Charles River Laboratories at 4-6 weeks of age. Once the flank tumors reached >50mm^3, they were surgically outfitted with jugular vein catheters by Dr. Clay Rouse at Duke University for intravenous, imaging-contrast delivery. The mice were randomly assigned a PPV dose for EPRO-imaging on Day 1. Because PPV has a biological half-life of ~1.5h, on Day 2, each mouse received another different dose of PPV [67]. Finally, on Day 3, mice received their final doses of PPV (i.e: mouse 1 received 2mg/kg on Day 1, 0mg/kg on Day 2 and 4mg/kg on Day 3). One mouse died due to PPV complications; on isoflurane, PPV can acutely decreases vascular compliance, leading to cardiovascular collapse [57].

The second mouse model is an autochthonous sarcoma model induced by intramuscular delivery of an adenovirus expressing Cre recombinase (Adeno-Cre) to activate a conditional Kras mutation and to delete both p53 alleles in LSL-KrasG12D; p53fl/fl (KP) mice. The laboratory of Dr. Yvonne Mowery provided the sarcoma model for imaging once the flank tumors were palpable. These mice were randomized and stratified via tumor volume into three groups: 0mg/kg PPV (n=4), 2mg/kg PPV (n=4) and 4mg/kg PPV (n=4). Two mice per group were excluded due to hardware and software-based EPRO-imaging complications (with the exception of one mouse that did not survive the 4mg/kg PPV injection). The EPROI contrast agent was delivered intra-tumorally, so no jugular vein catheters were needed.

All procedures were approved by the Duke Division of Laboratory Animal Resources and the Institutional Animal Care and Use Committee. Once imaging had been completed, all mice were humanely sacrificed.

Jugular Vein Cannulation Surgery

Jugular vein catheters and accessories were sourced from Instech Laboratories. The protocol for this surgery is well-described elsewhere [68]. Briefly, mice were anesthetized via 1-5% isoflurane in pure oxygen for the duration of the surgery. They were placed on a heated surgical field where they received 10mg/kg meloxicam for pain management and eye lubrication. The throat was shaved, and a small skin incision was made to one side of the midline of the ventral cervical area. Suture was used to ligate the cranial and caudal portions of the jugular vein. This caudal suture was preplaced but tied loosely around the vein. The cranial suture was placed the same way but this suture is tied securely to ligate the vein. The ends are left long to secure the cranial portion of the cannula. Tension was on the cranial suture to stabilize the vein, the vein was cut with micro-scissors, and the subsequent hole widened to accommodate the cannula. The heparinized-saline-filled cannula was introduced into the jugular vein and tied in place with the remaining suture lengths. Once blood is aspirated, a path from the shoulders to the catheter was made under the skin. The cannula was fed through this hole and secured with both an access port and two autoclips. The skin near the jugular vein was also closed with an autoclip. Bupivacaine (not exceeding 2mg/kg) was dropped along the incisions for additional analgesia. The mice were monitored and their catheters flushed daily with heparinized saline to ensure patency.

Papaverine delivery

Pharmaceutical-grade papaverine hydrochloride (PPV) was obtained and resuspended in sterile saline to obtain a 0.8mg/mL solution. It was injected intravenously via the retro-orbital cavity in isoflurane-anesthetized mice. Acute, labored breathing accompanied PPV injections. Two mice did not survive the vascular destabilization and subsequent cardiovascular events.

Electron Paramagnetic Resonance Oxygen Imaging

EPROI is a method for studying materials with unpaired electrons. This method has been widely applied to research for assessing absolute pO_2 values in tumor hypoxic regions. There are two unpaired electrons in oxygen molecule. When a magnetic field is applied, these two electrons are forced to be oriented either parallel or anti-parallel to the magnetic field [69]. Each alignment will absorb a specific energy [69]. Due to the Maxwell-boltzmann distribution, the unpaired electrons are more likely to distribute in the lower state [69]. The net energy between higher and lower state is the absorption that is monitored and converted to a spectrum [69].

Electron paramagnetic resonance oxygen imaging (EPROI) was performed to noninvasively quantify the tissue oxygen within tumor-bearing mouse flanks. The JIVA-25 EPROI machine was developed and loaned to Duke by O2M Technologies (Chicago, Il). Additionally, O2M sourced and provided the spin-probe trityl (OX063 and OX063-D24); trityl is a water-soluble, oxygen-reporting molecule that acts as a contrast agent for EPRO-imaging. For the E0771 tumor model, trityl was delivered via jugular vein cannulation at a rate of 150-300 μL/h at a 70mM concentration. For the sarcoma model, 3mM trityl was injected into the tumor into ~6 tracks for a total of ~250μL. All mice received a set of baseline images (pre-PPV) and post-PPV images (90min after PPV was injected). All mice were placed within a heated bed under 1-3% isoflurane with their tumors held in place with dental mold for imaging. The E0771 mice used the 19mm resonator; this diameter provides a high signalto-noise ratio similar to a MRI surface coil. The sarcoma mice used a 25mm resonator because their larger, intramuscular tumors caused over-coupling issues within the JIVA-25 when placed in the 19mm resonator. The proprietary Lab-View-based software, SpecMan4EPR, was used for image acquisition. An inversion recovery electron spin echo sequence was used for all image acquisitions. Generally, 3-5 images were acquired and averaged for a low-noise image.

3D, pO_2 images were reconstructed in Matlab (v 2020b). Regions-of-interest were made around either the E0771 tumor (the approximate location), the E0771 normal tissue (as far from the tumor as possible) or the large, central region of the sarcoma tumor. The mean and standard deviation tissue pO_2, along with the hypoxic fraction (<10mmHg), were recorded for each image. In order to compare the two mouse models and combine datasets, post-PPV values were normalized to baseline (pre-PPV), or the baseline values were subtracted from the post-PPV values. Due to small group sizes, no statistical analyses were performed.

3. Results

OCR, blood-flow rate, and arterial pO2 effects on hypoxia

Figure 5 shows that the hypoxic fraction changes with oxygen consumption rate. I select three ranges of oxygen conditions: < 10mmHg, < 6mmHg and < 4mmHg.

As the OCR increases, the hypoxic fraction increases across all conditions.

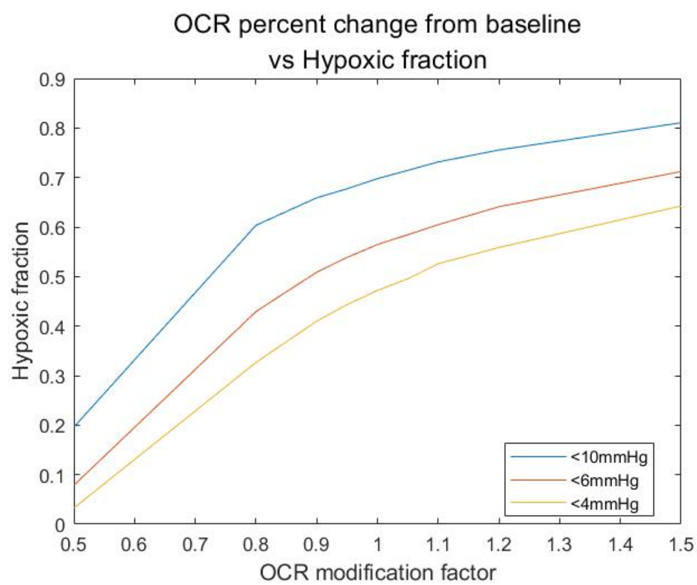

Figure 5: OCR percent change from baseline vs hypoxic fraction.

This figure shows the change in OCR from baseline for three hypoxic fractions: <10mmHg (blue line), <6mmHg (red line) and <4mmHg (yellow line). There is a non-linear relationship between increasing OCR and hypoxic fractions.

As shown in figure 6 and 7, which indicate the hypoxic fraction changes with OCR from 50% below baseline to 50% above baseline respectively.

As shown in figures 8 and 9, variations in blood-flow rate and arterial pO2 cause a decrease in the hypoxic fraction.

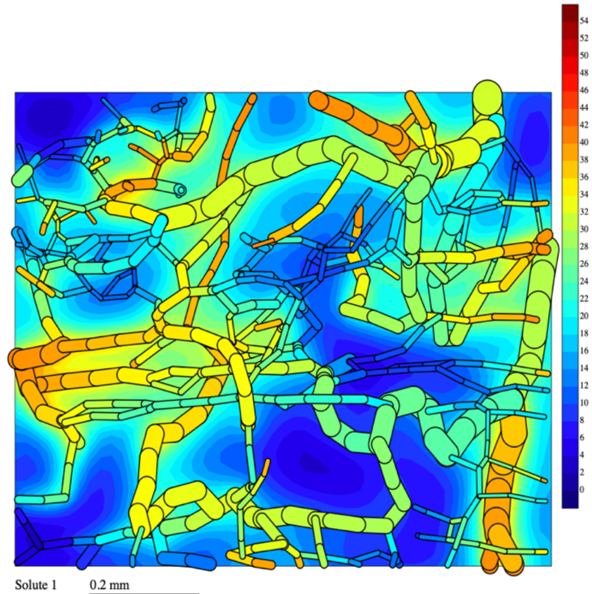

Figure 6: pO_2 map at OCR at 50% below baseline.

The color bar indicates pO_2 value from 0-54 mmHg. Blue region represents hypoxic regions.

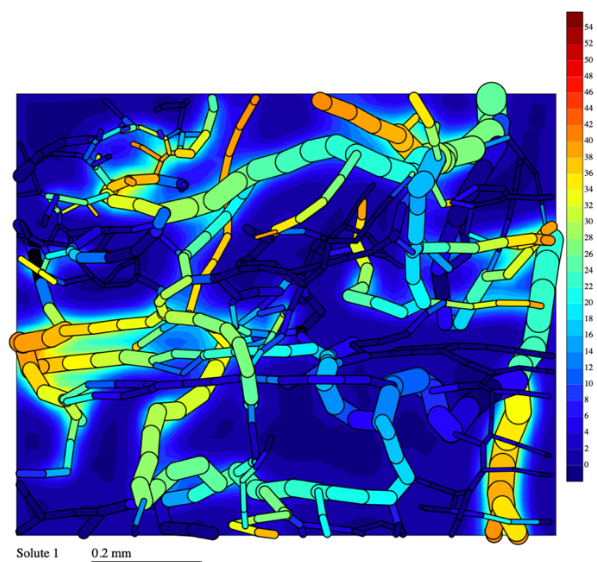

Figure 7: pO_2 map at OCR at 50% above baseline.

The color bar indicates pO_2 value from 0-54 mmHg. Blue region represents hypoxic regions.

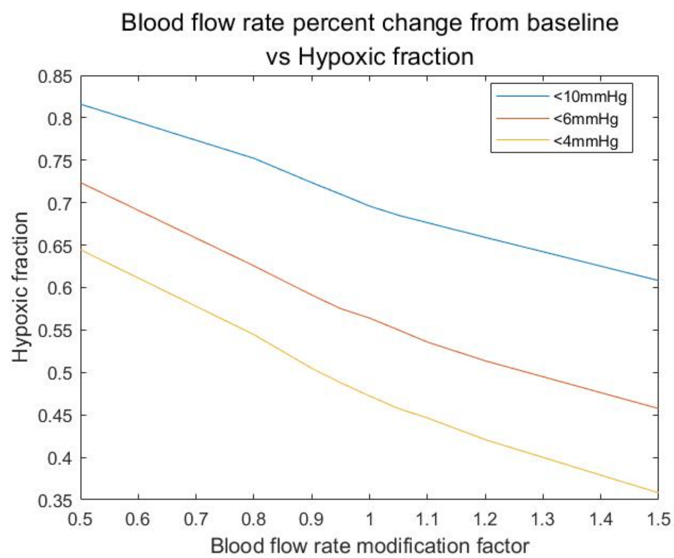

Figure 8: Blood-flow rate percent change from baseline vs hypoxic fraction.

This figure shows the change in blood flow rate percent change from baseline for three hypoxic fractions: <10mmHg (blue line), <6mmHg (red line), and <4mmHg (yellow line).

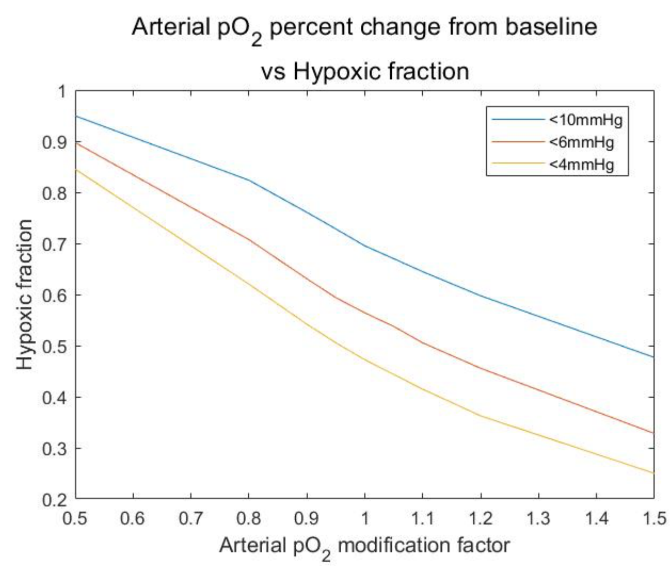

Figure 9: Arterial pO_2 percent change from baseline vs hypoxic fraction.

This figure shows the change in arterial pO_2 percent change from baseline for three hypoxic fractions: <10mmHg (blue line), <6mmHg (red line), and <4mmHg (yellow line).

Figure 10 shows the overall hypoxic fraction change with OCR (M), blood-flow rate (Q), and arterial pO_2 (P). The slope of OCR change is much steeper than either blood-flow rate or arterial pO_2. The hypoxic fraction becomes a constant after blood-flow rate and arterial pO_2 are increased around threefold. If the hypoxic fraction in the selected tissue is pO_2 <4 mmHg, the predicted hypoxic fraction in the simulation region is approximately 47%.

Figure 11 presents the spatial distribution that corresponds with OCR and arterial pO_2 variations. OCR rises from 50% below the baseline to 50% above the baseline. Arterial pO_2 increases from 50% below the baseline to 20% above the baseline. As expected, hypoxic fraction increases as OCR increases. On the contrary, a negative correlation is found between arterial pO_2 and hypoxic fraction.

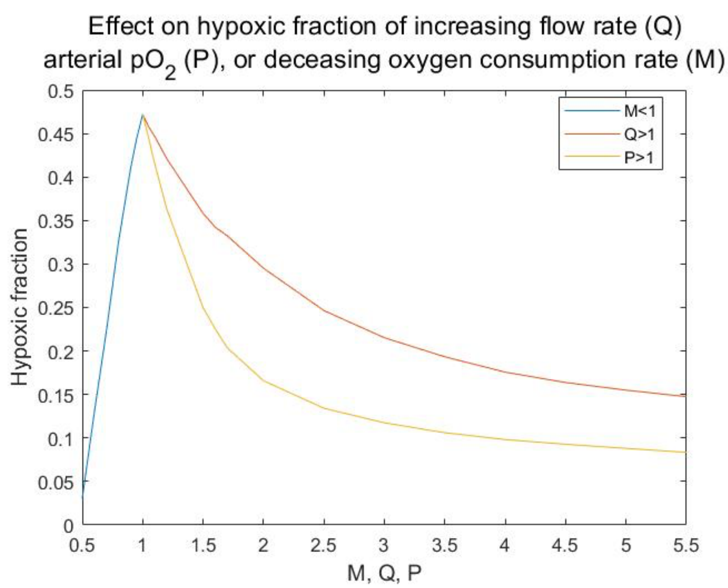

Figure 10: Effect on hypoxic fraction of increasing flow rate (red line), arterial pO_2 (yellow line), or decreasing oxygen consumption rate (blue line).

Arterial pO_2 =100 mmHg, blood flow rate = 8×10^{-7} cm^3/s, maximum oxygen consumption rate= 4.5 cm^3 O_2/100g/min.

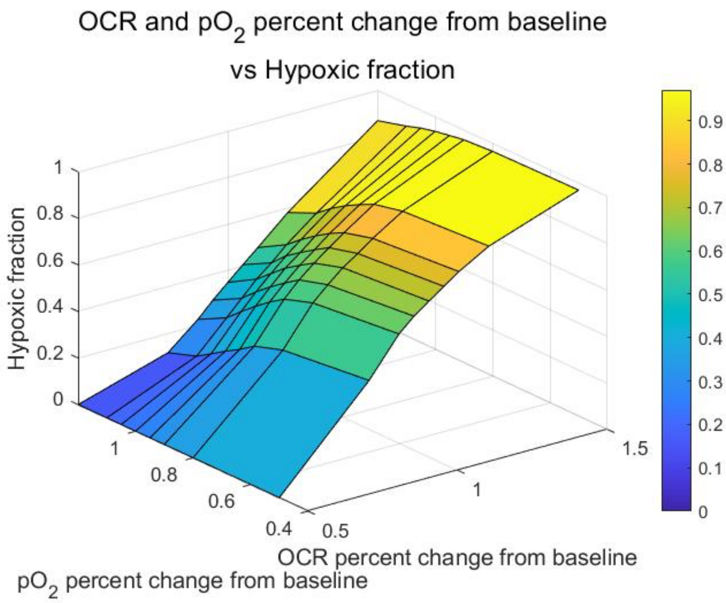

Figure 11: Hypoxic fraction contour vs OCR and Arterial pO_2 change.

This figure shows the hypoxic fraction (Z-axis) change with simultaneous OCR (X-axis), and oxygen supply (Y-axis) change. OCR changes from below 50% from baseline to above 50%. Oxygen supply changes from below 50% from baseline to 20% above.

Papaverine effects on hypoxia

According to published data, papaverine can decrease OCR in tumor regions significantly in a dose-dependent manner and thus to radiosensitize solid tumors[57]. In my results, figure 12 shows the mean pO_2 values in E0771 (A) and sarcoma tumor models (B). In these two tumor models, 2 mg/kg papaverine causes a significant rise in pO_2 levels. However, addition of 4 mg/kg papaverine results in different pO_2 changes in these two tumor models.

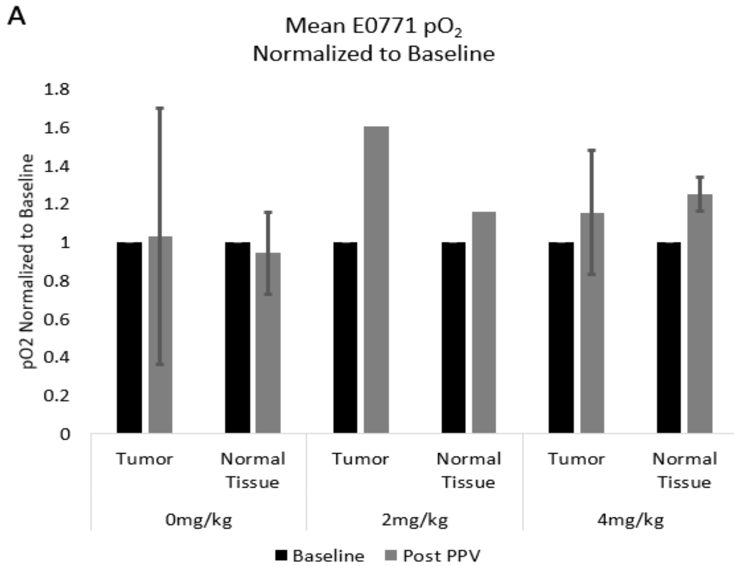

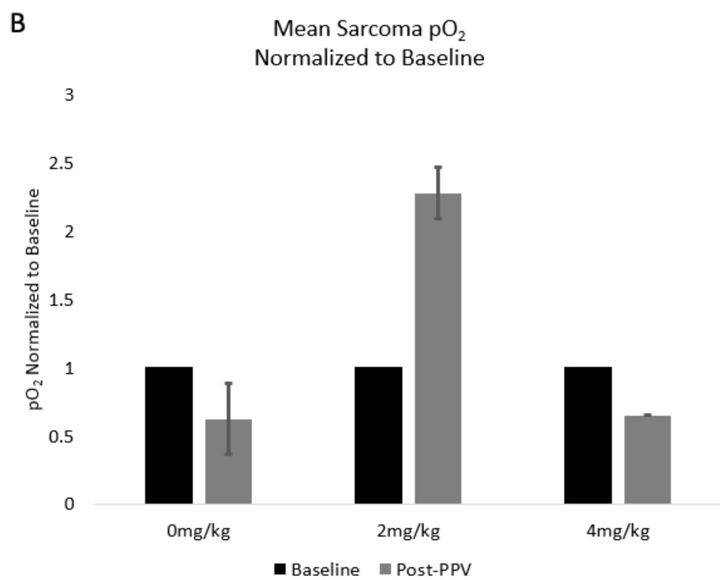

Figure 12: Tissue pO_2 values before and after papaverine delivery, normalized to the baseline image.

(A) For the E0771 tumor model, two, 3D regions-of-interest were analyzed: normal tissue and tumor tissue. The results between two mice were averaged with the standard deviation after the values were normalized to the baseline value. Note that there is only one mouse for the 2mg/kg group due to a mouse succumbing to surgical complications prior to the experiment. (B) The pO_2 data is shown here for the sarcoma

tumor model. This tumor is grown intramuscularly, so the central region of the leg was analyzed for changes in tissue pO_2 due to papaverine. Note, due to imaging-hardware malfunctions, there is only one mouse in the 4mg/kg group. Figure courtesy of Ashlyn Rickard.

Figure 13 presents the papaverine effects on hypoxic fractions in E0771 (A) and sarcoma (B) tumor models. As expected, at 2 mg/kg, papaverine can decrease hypoxic fractions dramatically. At 4 mg/kg, hypoxia increases a lot in E0771 cells but very slightly in sarcoma model.

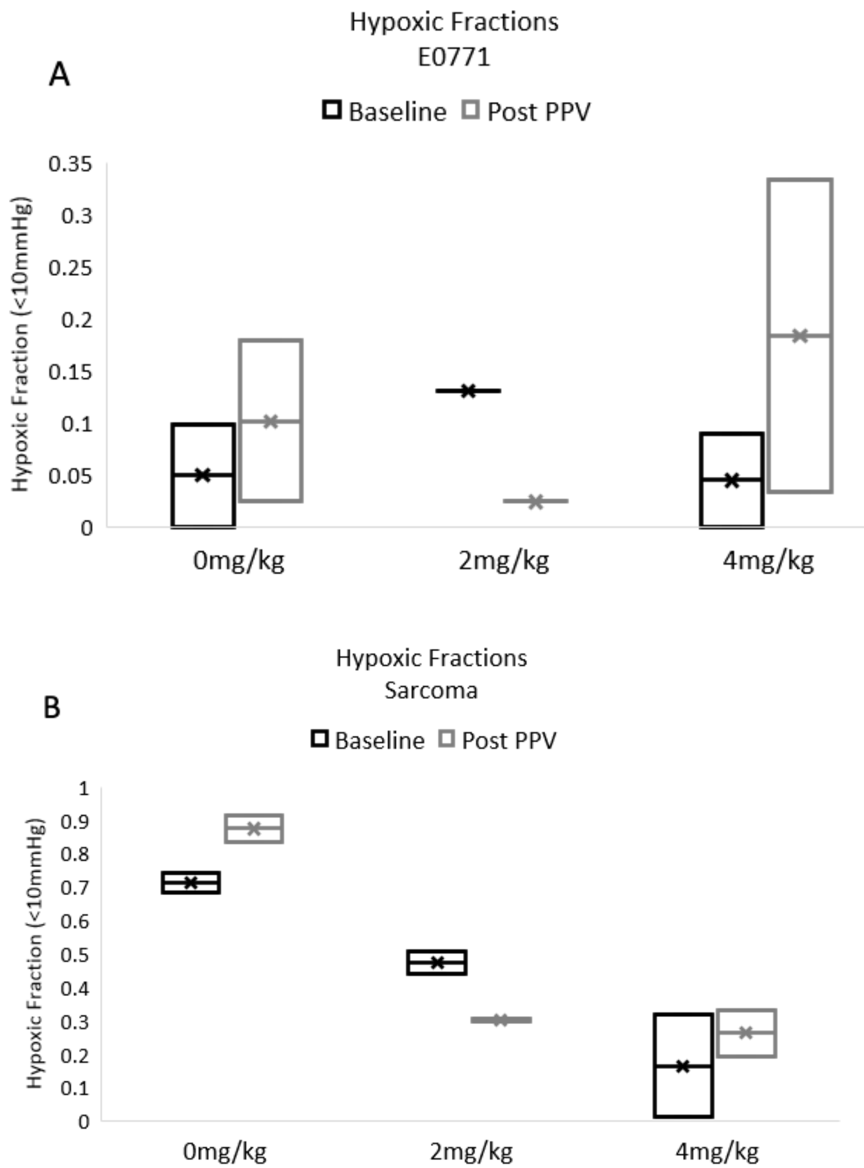

Figure 13: Hypoxic fractions (<10mmHg) in E0771 and sarcoma tumor models before and after papaverine injection.

(A) For the E0771 tumor, the fraction of hypoxic cells (cells less than 10mmHg) is shown for all three papaverine-dose groups. Baseline values (pre-PPV) are shown in black, while post-PPV groups are shown in gray. Each group has n=2 mice except for 2mg/kg which has one mouse. (B) For the sarcoma tumor, the fraction of hypoxic cells (cells less than 10mmHg) is shown for all three papaverine-dose groups. Baseline values (pre-PPV) are shown in black, while post-PPV groups are shown in gray. Each

group has n=2 mice except for 4mg/kg which has one mouse. Figure courtesy of Ashlyn Rickard.

Figure 14 and 15 show the EPRO images before and after papaverine delivery in E0771 and sarcoma tumor models respectively. In these two tumor models, addition of 2 mg/kg papaverine causes most parts of hypoxia disappeared. However, in some areas with high oxygen content in the 4 mg/kg group, addition of papaverine decreases oxygen content.

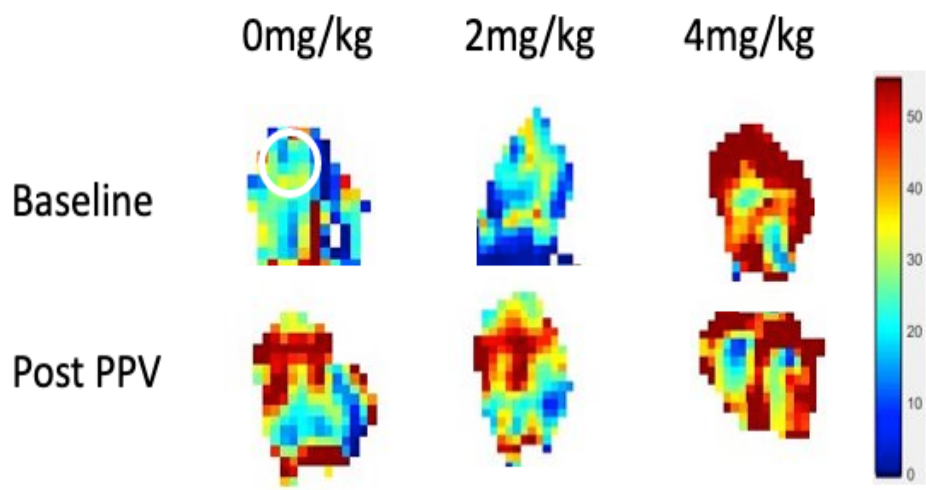

Figure 14: E0771 EPRO images before and after papaverine delivery.

These EPRO images show the axial view of the leg with the tumor before and after 0mg/kg, 2mg/kg and 4mg/kg papaverine doses. The baseline image for 0mg/kg shows an example tumor ROI in the white circle. The color bar indicates the range of 0-55mmHg where dark blue represents hypoxic regions in the tumor and surrounding leg. All images are from the same mouse across 3 days. Figure courtesy of Ashlyn Rickard.

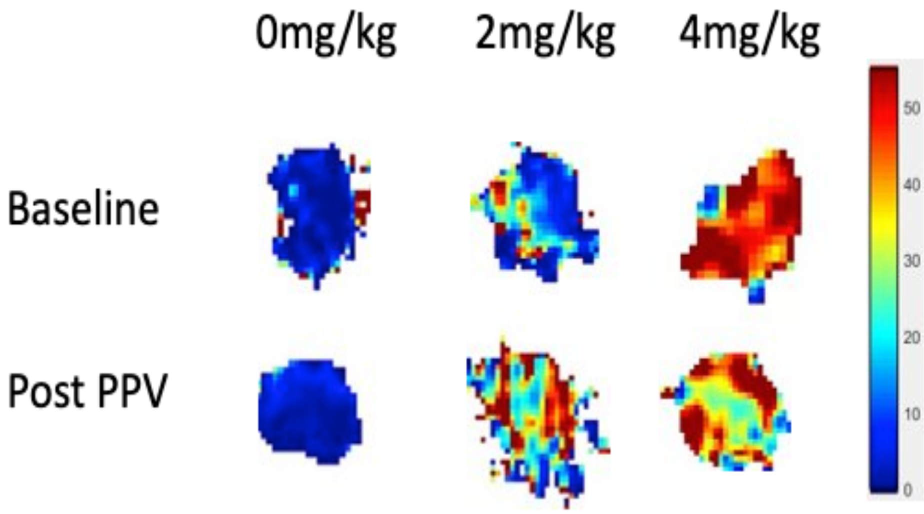

Figure 15: Sarcoma EPRO images before and after papaverine delivery.

These EPRO images show the axial view of the leg with the intra-muscular tumor before and after 0mg/kg, 2mg/kg and 4mg/kg papaverine doses. The color bar indicates the range of 0-55mmHg where dark blue represents hypoxic regions in the tumor and surrounding leg. Each PPV dose (baseline and post-PPV) images are from a different mouse. Figure courtesy of Ashlyn Rickard.

4. Discussion

Modification of OCR is effective to reduce hypoxia

The simulation illustrates that higher arterial pO_2 and lower OCR are conducive for decreasing the hypoxic fraction. Additionally, modification of OCR is more effective to reduce hypoxic fraction than modification of blood flow rate and arterial pO_2 since the hypoxic fraction varies more dramatically when OCR is changed. A 30% reduction in oxygen consumption rate leads to 21% reduction in the hypoxic fraction. However, a 30% increase in blood-flow rate and arterial pO_2 result in 6% and 13% reduction in hypoxic fraction respectively. A 20% reduction in oxygen consumption rate plus a 20% increase in arterial pO_2 causes a 40% decrease in hypoxia. Put simply, the hypoxic fraction is more sensitive to OCR changes.

Benej et al. concluded that the FDA-approved drug papaverine can effectively reduce OCR without many side effects and thus improve radiation response [57]. His group tested papaverine *in vitro* in both cancer cells (E0771 cells) and normal cells. The results showed that papaverine can decrease OCR dramatically (~30% decrease) in the first 30-50min regardless of whether the cells are normal or tumor cells. In reality, increasing neither arterial pO_2 nor blood flow rate to over threefold is technologically difficult to implement. To some extent, modification of OCR to reduce hypoxic fraction is a better approach.

Boundary condition affects hypoxic fraction prediction

When I compare my results with previously published data [61], the parameter differences are listed in table 2. In my results, the hypoxic fraction reaches a plateau after blood flow rate and oxygen supply have a 3-fold increase. In published data [61], hypoxia is totally abolished by a 4-times increase in blood flow rate and around 11 times increase in arterial pO_2 (Figure 16). The reason for this may be the difference in boundary conditions. In published data [61], an upstream region is assumed. They consider the simulated region first passes through other tissue then to the simulation region. However, in my simulation, I suppose the region is an infinite domain. The selected network is embedded in the region where the net exchange of oxygen across the region boundaries is zero. In my simulation, the hypoxic fraction is the region where pO_2 value less than 4 mmHg, which is less than 3 mmHg in the published research (Figure 10). In the control state, the hypoxic fraction is 47% and 34% in my simulation and published paper respectively.

Table 2: Parameter differences between my simulation and published paper [61]

Parameter	Our	Dr. Secomb
OCR range	0.00025-0.00075 cm^3 O_2/g/s	0.00028-0.0004 cm^3 O_2/g/s
Flow rate range	0.0868-0.2605 (multiplicative value)	$(0.2\text{-}5)\times10^{-7}$ cm^3/s
Hypoxic fraction	pO_2 <4 mmHg	pO_2 <3 mmHg
Boundary condition	Infinite domain (do not include an “upstream region”)	Include an “upstream region”

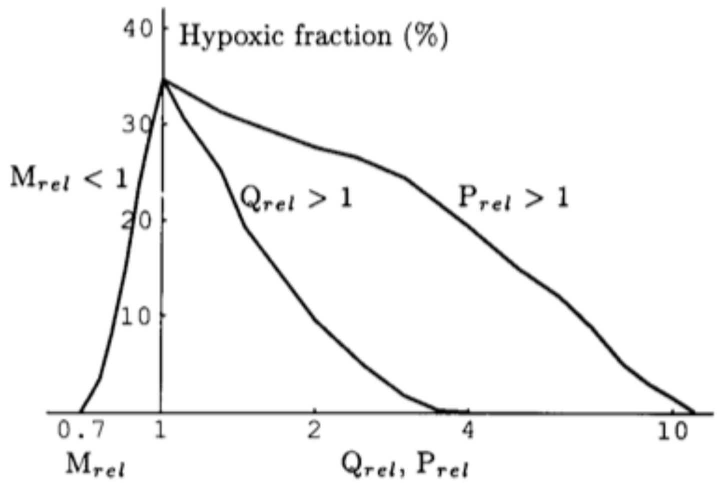

Figure 16: Effect on hypoxic fraction of OCR, flow rate and oxygen supply.

Arterial pO_2 =100 mmHg, blood flow =8×10^{-7} cm^3/s and maximal consumption =2.4 cm^3 O_2/100g/min [61]. The simulated hypoxic fraction on this occasion is 34%.

In the study by Secomb et al published in 2004, they compared the effects of different prediction methods of hypoxia [38]. They applied Green's function to simulate pO_2 values in tumor, brain, and skeletal muscle tissue. Their results indicate that compared with pointwise no-flux solution, both net no-flux and infinite-domain solution cause reduced hypoxic fraction [66]. Therefore, the boundary condition is related to the result of hypoxic fraction prediction.

pO_2 maps change with OCR, blood-flow rate, and oxygen supply

In Appendix A and B, I present the pO_2 maps of decreasing OCR and blood-flow rate respectively. With the decrease of OCR, the blue regions which represent hypoxic fraction become lighter and smaller. Conversely, in the pO_2 maps with decreasing blood-flow rate, these hypoxic regions become more hypoxic (dark blue becomes darker). In Appendix A and B, although reduction of OCR and blood-flow rate can reduce overall hypoxic fraction, there are still some pockets of hypoxia such as the corners where there is not enough vasculature. Besides, small arterials are nearly independent of OCR and blood-flow rate since these areas are always hypoxic. Appendix C shows the pO_2 maps at increasing arterial pO_2. This map shows that the hypoxic fraction decreases when oxygen supply decreases. In addition, compared with the previous two maps, arterial oxygen levels vary more obviously. However, in the regions where is poor vascularized or in small arterials, increase of oxygen supply is limited to reduce hypoxia.

Papaverine effects on the hypoxic fraction

In the paper published by Hang Huang from the Southern Medical University in 2008, they investigated the papaverine functions in human prostate cancer cell (PC-3) and normal human fibroblast (NHF) cells. The results demonstrated that papaverine has selective antiproliferative effects in PC-3 cells and NHF cells (Figure 17). Low doses of papaverine can decrease cell viability to 65% in 24hr while reduce the oxygen consumption rate by half [50].

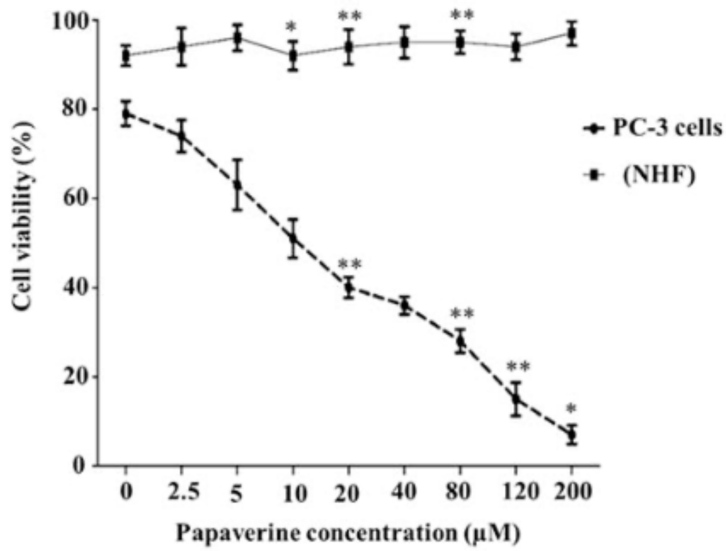

Figure 17: Papaverine effects in human prostate cancer cell (PC-3) and normal human fibroblasts [50].

Papaverine presents selective antiproliferative effects in PC-3 cells and NHF cells.

In Benej's 2018 paper, papaverine as an inhibitor of mitochondrial complex I, was proved to reduce OCR significantly and thus to radiosensitize solid tumors [57]. In figure 1, papaverine decreases OCR dramatically in the first 30-40 min compared with control state.

In our results, as shown in figure 18, papaverine makes effects on hypoxia or OCR also in a dose-dependent manner. Low dose papaverine (2 mg/kg) causes around 18 mmHg pO_2 increase. Compared with Green's model, around 17% OCR decrease can reflect the same amount of increase in tumor pO_2 at 2mg/kg. When the dose of papaverine is increased to 4 mg/kg, pO_2 level drops a lot compared to 2 mg/kg. Hypoxic fraction rises to a level close to the initial baseline when no papaverine is added.

Actually, PPV can decrease OCR and widen blood vessels simultaneously. There is a competing effect between decreasing OCR and vasodilation. PPV can lower the perfusion in the tissue and thus reduce the blood-flow rate. At 4mg/kg, when the tumor pO_2 decreases after PPV addition, the vasodilation effect is stronger than OCR decrease. In this condition, the OCR effect is minimal. In Green's function method, a 22% decrease in blood-flow rate would result in a similar decrease in tumor pO_2 at 4 mg/kg.

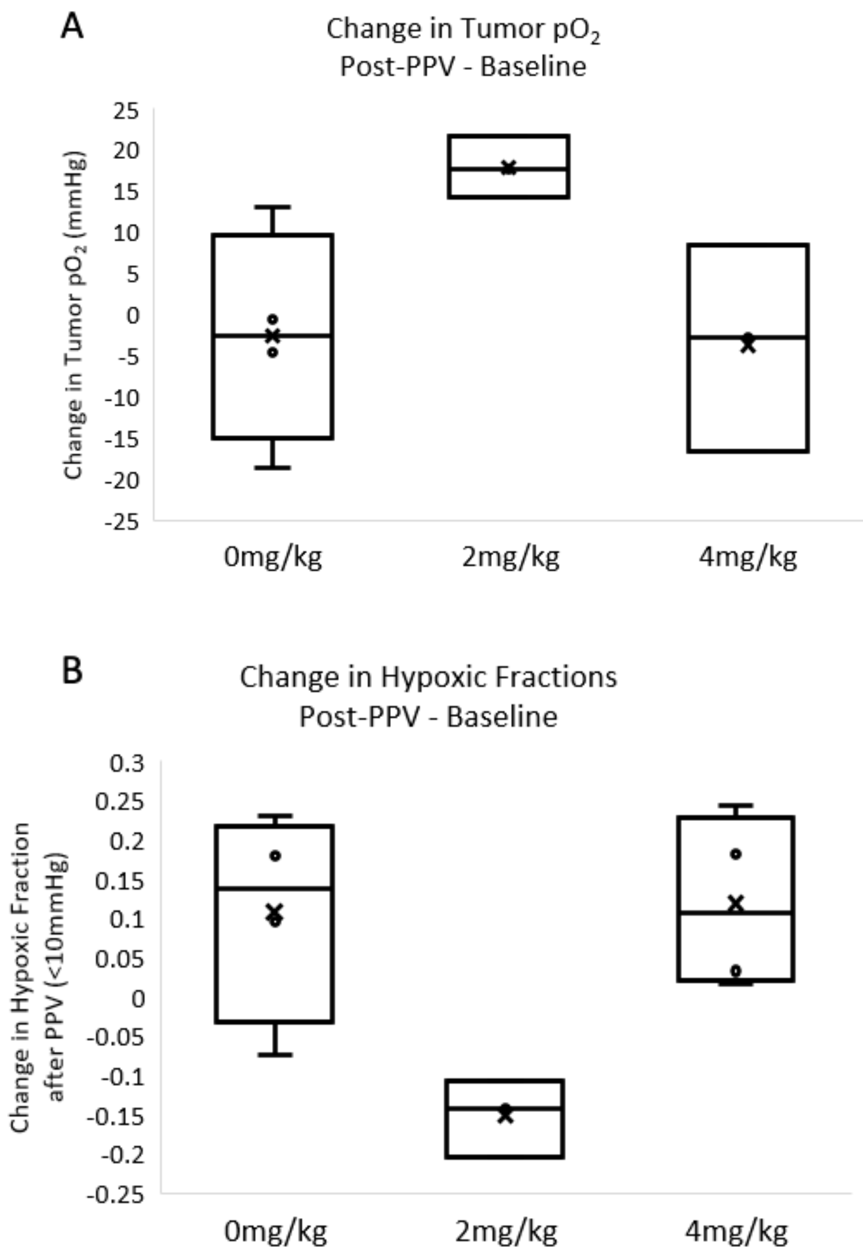

Figure 18: Change in pO_2 and the hypoxic fraction (<10mmHg) across all tumor models.

(A) and (B) By subtracting the baseline tumor data from the post-PPV data in the same tumor region, all tumor models are comparable across all papaverine-dose

groups. There is n=4 mice in the 0mg/kg group, n=3 mice in the 2mg/kg group and n=3 mice in the 4mg/kg group. Figure courtesy of Ashlyn Rickard.

5. Conclusion

The Green's function method offers a reasonable simulation of oxygen delivery in tissue by vascular networks. However, the simulation presented here is for one selected vascular configuration. As for other geometries, such as more sparsely distributed configuration, this method cannot offer an absolute answer without a tumor from which to model the sparse vasculature.

My results support previously published work [61]. The hypoxic fraction is proportional to blood-flow rate and arterial pO_2. On the contrary, hypoxic fraction is negatively correlated with oxygen consumption rate. Hypoxia is more sensitive to oxygen consumption rate variations. In reality, increasing blood flow rate and oxygen supply to over 3-fold from baseline is difficult to implement. As a result, to reduce the hypoxic fraction in human solid tumors, modification of oxygen consumption rate is an efficient way. Papaverine as an FDA-approved drug is an ideal clinical radiosensitizer to improve radiation response by decreasing oxygen consumption rate.

For further improvement, more mice are needed to get a more accurate animal result. In addition, the results in this research are only for one geometry, we cannot generalize to other geometries.

Appendix A

Appendix A presents the pO_2 maps that changes with OCR. OCR gets smaller from (1) to (9). In each figure, the color bar represents pO_2 values from 0 mmHg to 54 mmHg. Dark blue represents hypoxic regions.

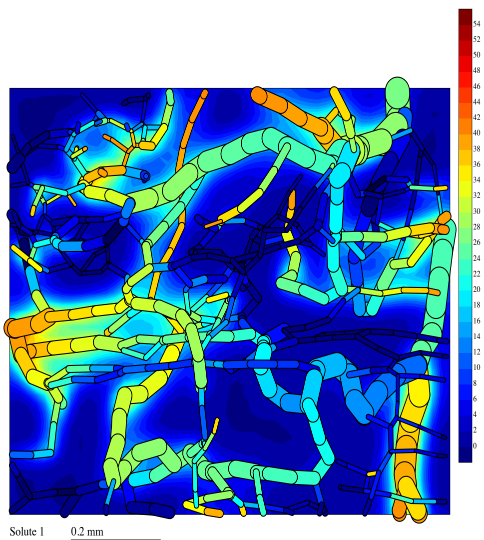

(1)

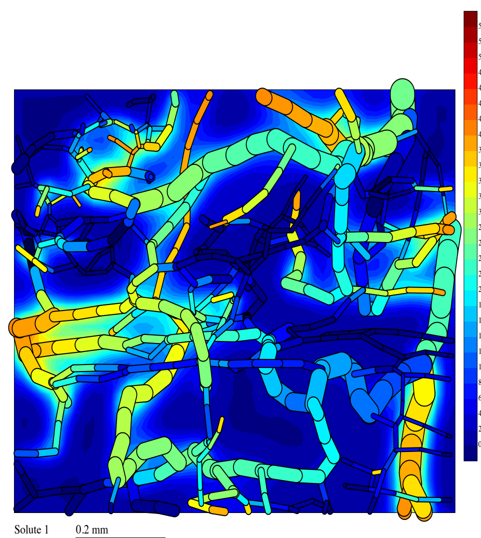

(2)

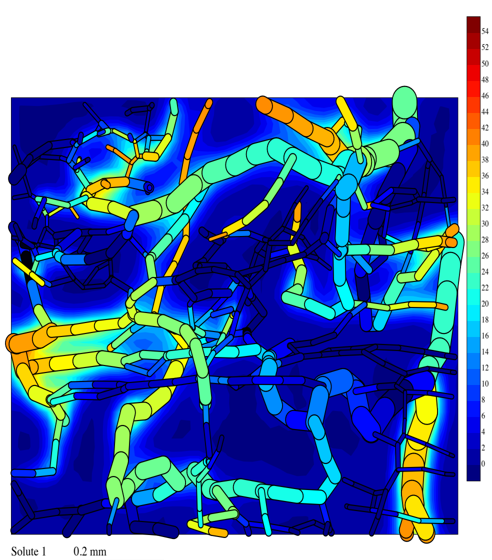

(3)

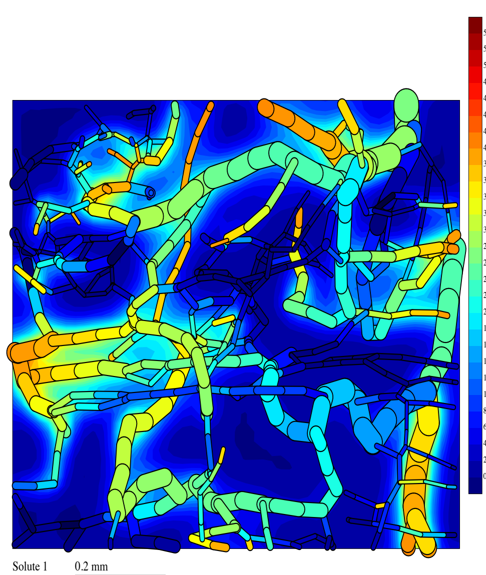

(4)

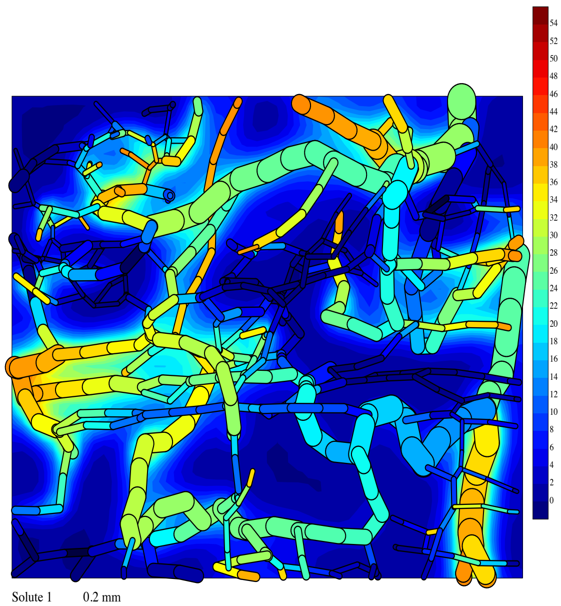
54 52 50 48 46 44 42 40 38 36 34 32 30 28 26 24 22 20 18 16 14 12 10 8 6 4 2 0
Solute 1
0.2 mm

(5)

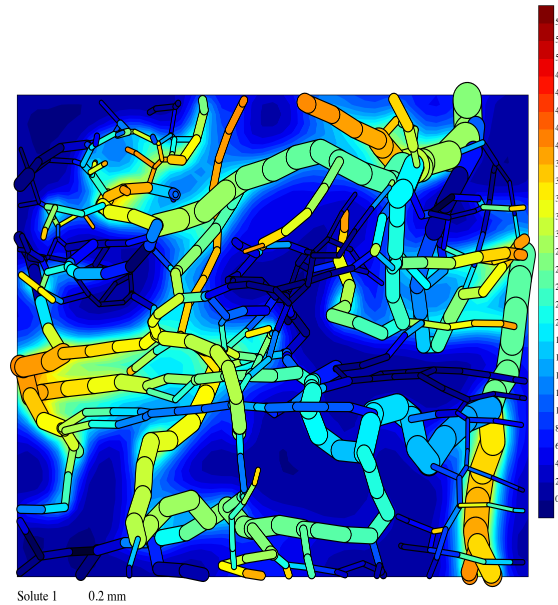
54 52 50 48 46 44 42 40 38 36 34 32 30 28 26 24 22 20 18 16 14 12 10 8 6 4 2 0
Solute 1
0.2 mm

(6)

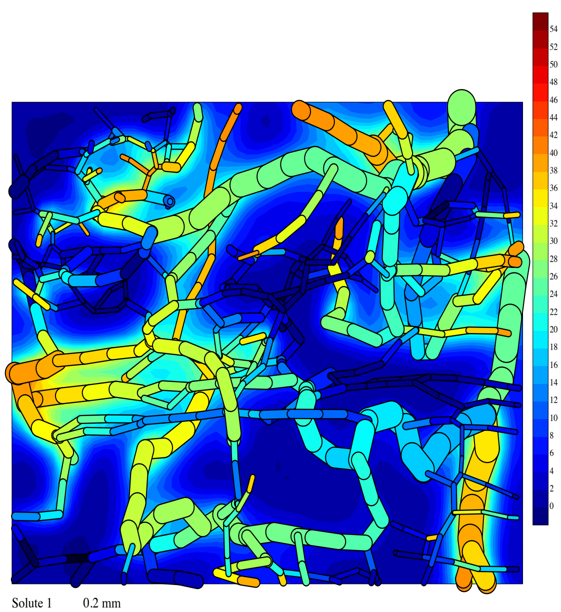
54 52 50 48 46 44 42 40 38 36 34 32 30 28 26 24 22 20 18 16 14 12 10 8 6 4 2 0
Solute 1
0.2 mm

(7)

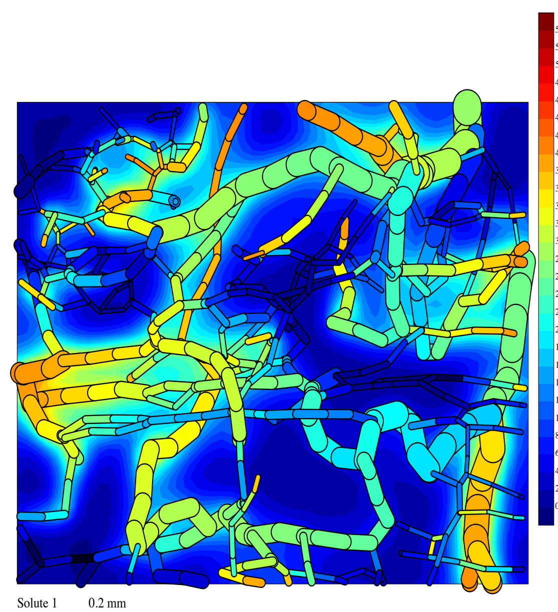
54 52 50 48 46 44 42 40 38 36 34 32 30 28 26 24 22 20 18 16 14 12 10 8 6 4 2 0
Solute 1
0.2 mm

(8)

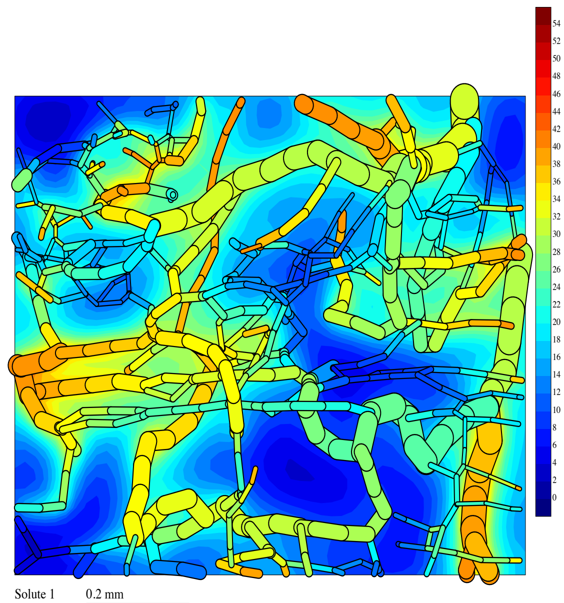
Solute 1
0.2 mm
54
52
50
48
46
44
42
40
38
36
34
32
30
28
26
24
22
20
18
16
14
12
10
8
6
4
2
0

(9)

Appendix B

Appendix B presents the pO_2 maps that changes with blood-flow rate. Blood-flow rate gets smaller from (1) to (9). In each figure, the color bar represents pO_2 values from 0 mmHg to 54 mmHg. Dark blue represents hypoxic regions.

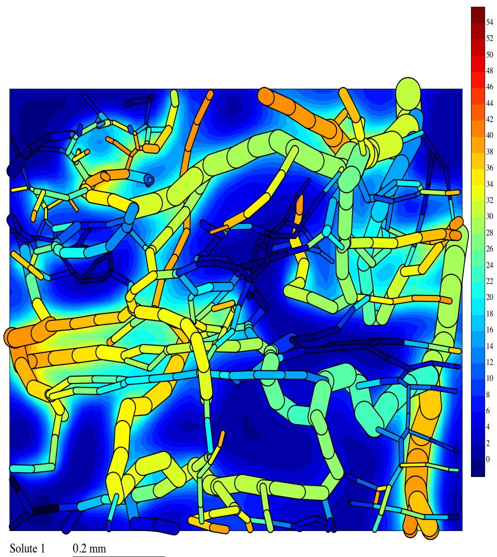

(1)

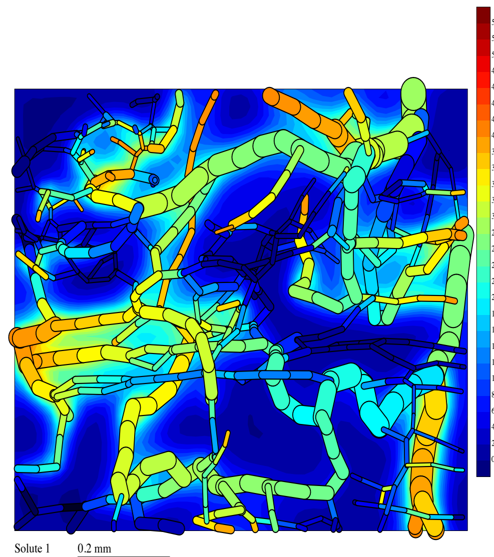

(2)

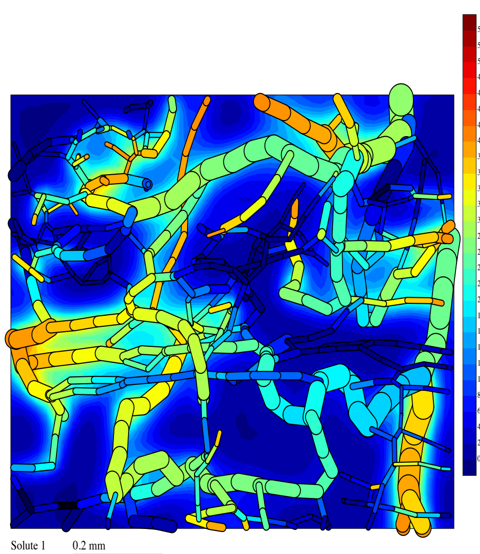

(3)

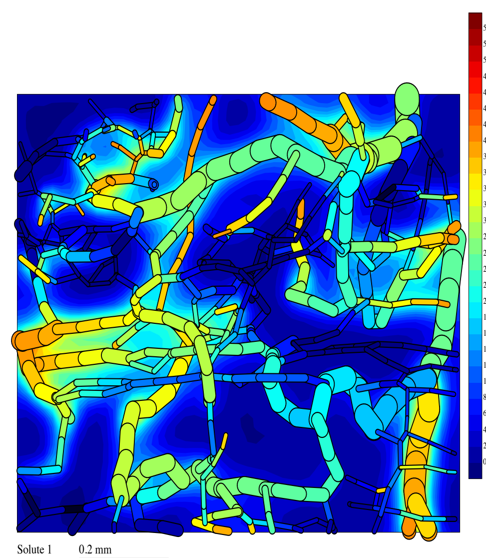

(4)

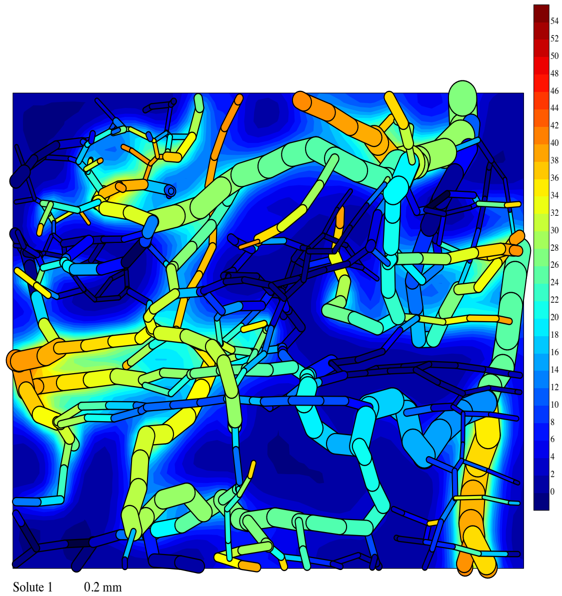
Solute 1
0.2 mm
54
52
50
48
46
44
42
40
38
36
34
32
30
28
26
24
22
20
18
16
14
12
10
8
6
4
2
0

(5)

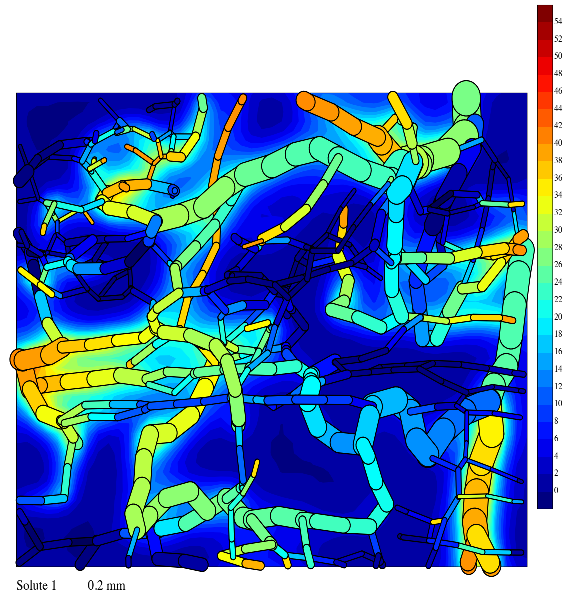
Solute 1
0.2 mm
54
52
50
48
46
44
42
40
38
36
34
32
30
28
26
24
22
20
18
16
14
12
10
8
6
4
2
0

(6)

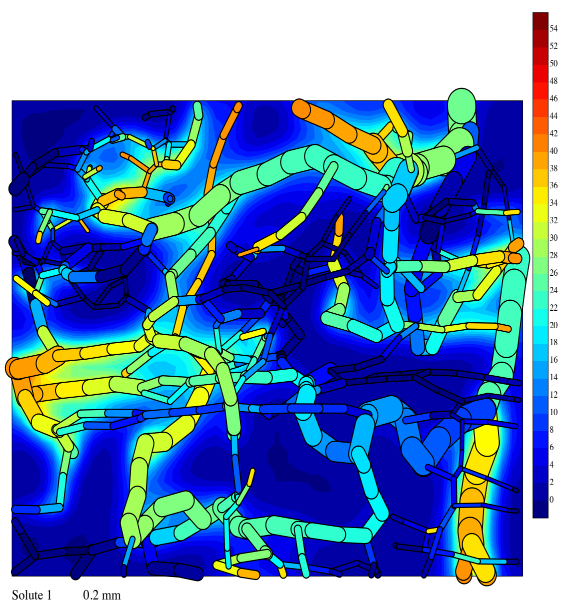
Solute 1
0.2 mm
54
52
50
48
46
44
42
40
38
36
34
32
30
28
26
24
22
20
18
16
14
12
10
8
6
4
2
0

(7)

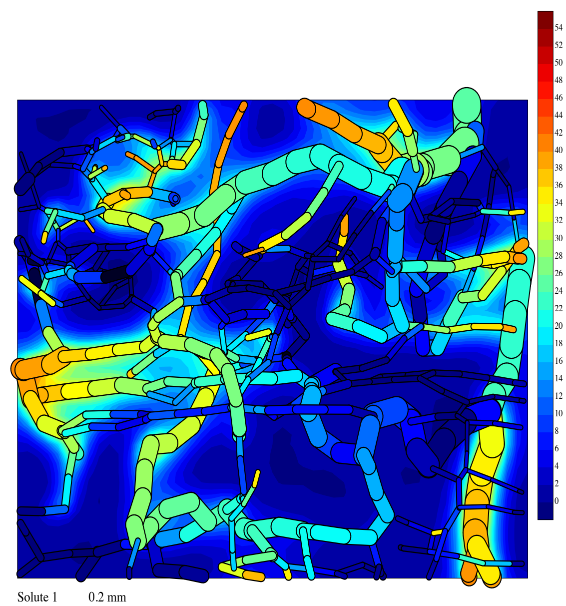
Solute 1
0.2 mm
54
52
50
48
46
44
42
40
38
36
34
32
30
28
26
24
22
20
18
16
14
12
10
8
6
4
2
0

(8)

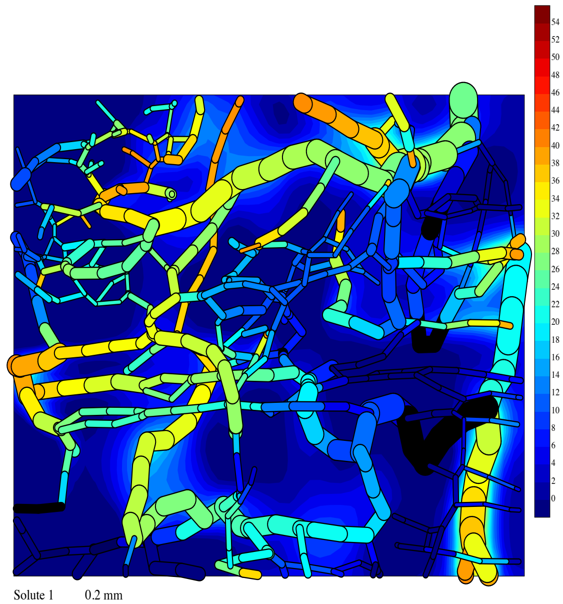
54
52
50
48
46
44
42
40
38
36
34
32
30
28
26
24
22
20
18
16
14
12
10
8
6
4
2
0
Solute 1
0.2 mm

(9)

Appendix C

Appendix C presents the pO_2 maps that changes with arterial pO_2. Arterial pO_2 gets higher from (1) to (9). In each figure, the color bar represents pO_2 values from 0 mmHg to 54 mmHg. Dark blue represents hypoxic regions.

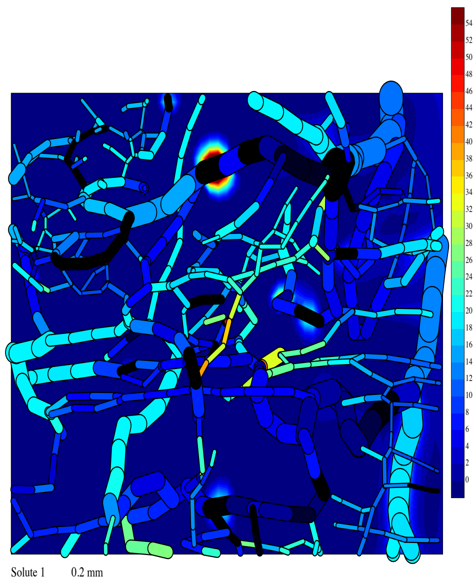

(1)

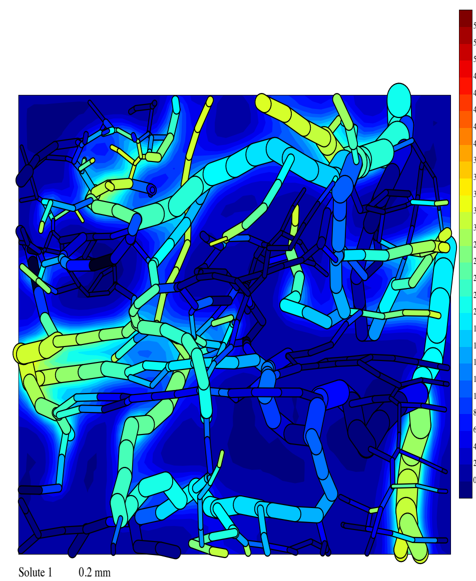

(2)

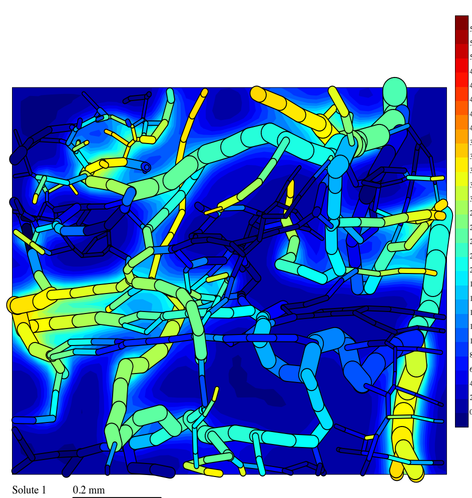

(3)

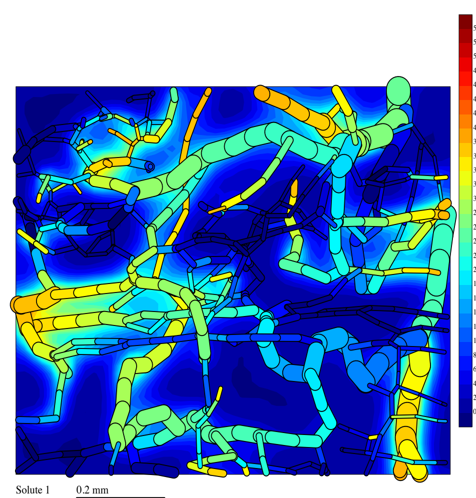

(4)

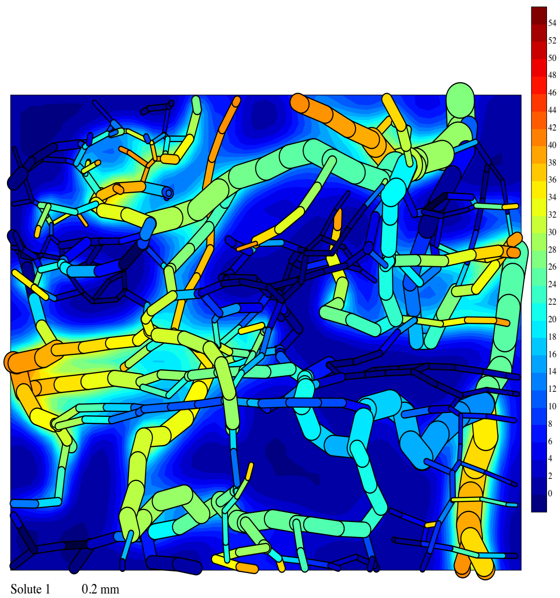
0
2
4
6
8
10
12
14
16
18
20
22
24
26
28
30
32
34
36
38
40
42
44
46
48
50
52
54
Solute 1
0.2 mm

(5)

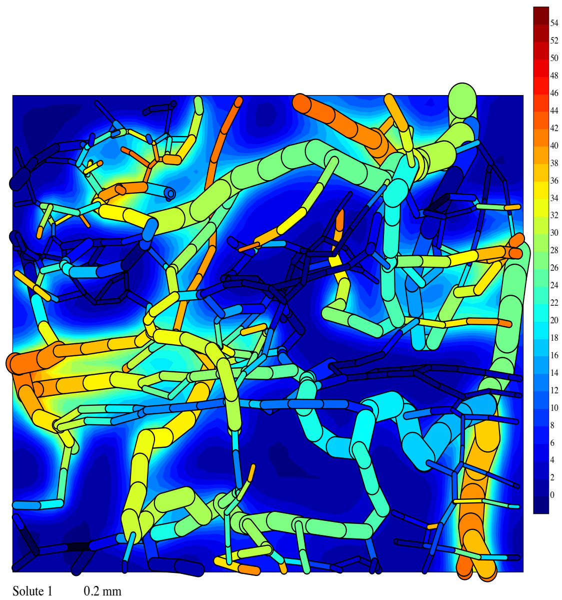
0
2
4
6
8
10
12
14
16
18
20
22
24
26
28
30
32
34
36
38
40
42
44
46
48
50
52
54
Solute 1
0.2 mm

(6)

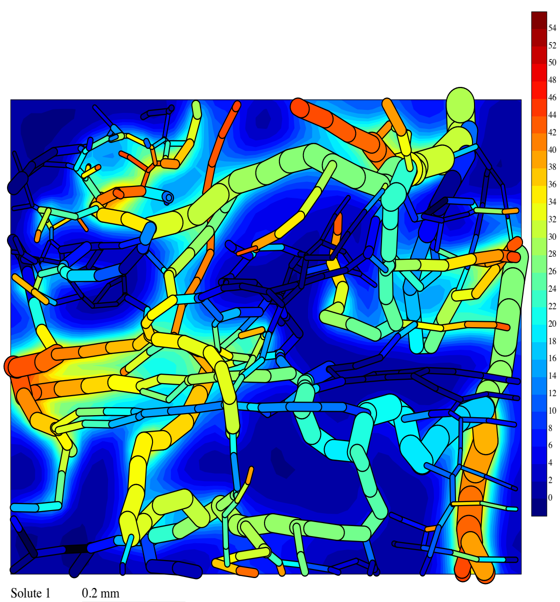
0
2
4
6
8
10
12
14
16
18
20
22
24
26
28
30
32
34
36
38
40
42
44
46
48
50
52
54
Solute 1
0.2 mm

(7)

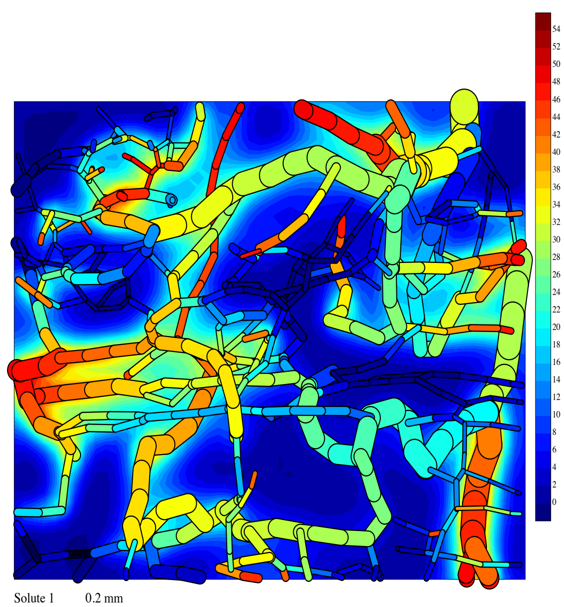
0
2
4
6
8
10
12
14
16
18
20
22
24
26
28
30
32
34
36
38
40
42
44
46
48
50
52
54
Solute 1
0.2 mm

(8)

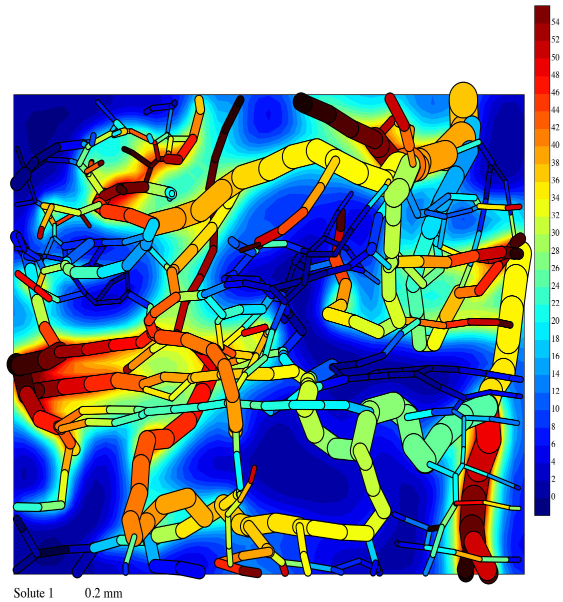

54
52
50
48
46
44
42
40
38
36
34
32
30
28
26
24
22
20
18
16
14
12
10
8
6
4
2
0
Solute 1
0.2 mm

(9)

References

[1] Schwartz, G. (1909). Ueber Desensibilisierung gegen rontgen und radiumstrahlen. *Munchener Medizinische Wochenschrift*, *24*, 1-2.

[2] Gray, L. H., Conger, A., Ebert, M., Hornsey, S., & Scott, O. C. A. (1953). The concentration of oxygen dissolved in tissues at the time of irradiation as a factor in radiotherapy. *The British journal of radiology*, *26*(312), 638-648.

[3] Lanzen, J., Braun, R. D., Klitzman, B., Brizel, D., Secomb, T. W., & Dewhirst, M. W. (2006). Direct demonstration of instabilities in oxygen concentrations within the extravascular compartment of an experimental tumor. *Cancer research*, *66*(4), 2219-2223.

[4] Kimura, H., Braun, R. D., Ong, E. T., Hsu, R., Secomb, T. W., Papahadjopoulos, D., ... & Dewhirst, M. W. (1996). Fluctuations in red cell flux in tumor microvessels can lead to transient hypoxia and reoxygenation in tumor parenchyma. *Cancer research*, *56*(23), 5522-5528.

[5] Dewhirst, M. W. (2018). A potential solution for eliminating hypoxia as a cause for radioresistance. *Proceedings of the National Academy of Sciences*, *115*(42), 10548-10550.

[6] Davidson, I. C., Sanger, C., & Thomlinson, R. H. (1955). High-pressure oxygen and radiotherapy. *The Lancet*, *265*(6874), 1091-1095.

[7] Du Sault, L. A. (1963). The effect of oxygen on the response of spontaneous tumours in mice to radiotherapy. *The British journal of radiology*, *36*(430), 749-754.

[8] Feldmeier, J. J. (2004). Hyperbaric oxygen for delayed radiation injuries. *Undersea Hyperb Med*, *31*(1), 133-45.

[9] Bergsjø, P., & Kolstad, P. (1968). Clinical trial with atmospheric oxygen breathing during radiotherapy of cancer of the cervix. *Scandinavian Journal of Clinical and Laboratory Investigation*, *21*(sup106), 167-171.

[10] Harrison, L. B., Chadha, M., Hill, R. J., Hu, K., & Shasha, D. (2002). Impact of tumor hypoxia and anemia on radiation therapy outcomes. *The oncologist*, *7*(6), 492-508.

[11] Snyder, S. A., Lanzen, J. L., Braun, R. D., Rosner, G., Secomb, T. W., Biaglow, J., ... & Dewhirst, M. W. (2001). Simultaneous administration of glucose and hyperoxia gas achieves greater improvement in tumor oxygenation than hyperoxia gas alone. *International Journal of Radiation Oncology* Biology* Physics*, *51*(2), 494-506.

[12] Adams, G. E., & Cooke, M. S. (1969). Electron-affinic Sensitization: I. A Structural Basis for Chemical Radiosensitizers in Bacteria. *International Journal of Radiation Biology and Related Studies in Physics, Chemistry and Medicine*, *15*(5), 457-471.

[13] Overgaard, J. (1989). Sensitization of hypoxic tumour cells—clinical experience. *International journal of radiation biology*, *56*(5), 801-811.

[14] Calais, G., & Hirst, D. G. (1991). In situ tumour radio sensitization induced by clofibrate administration: single dose and fractionated studies. *Radiotherapy and Oncology*, *22*(2), 99-103.

[15] Kjellen, E., Joiner, M. C., Collier, J. M., Johns, H., & Rojas, A. (1991). A therapeutic benefit from combining normobaric carbogen or oxygen with nicotinamide in fractionated X-ray treatments. *Radiotherapy and Oncology*, *22*(2), 81-91.

[16] Biaglow, J. E., Manevich, Y., Leeper, D., Chance, B., Dewhirst, M. W., Jenkins, W. T., ... & Evans, S. M. (1998). MIBG inhibits respiration: potential for radio-and hyperthermic sensitization. *International Journal of Radiation Oncology* Biology* Physics*, *42*(4), 871-876.

[17] Collingridge, D. R., & Rockwell, S. (2000). Pentoxifylline improves the oxygenation and radiation response of BA1112 rat rhabdomyosarcomas and EMT6 mouse mammary carcinomas. *International journal of cancer*, *90*(5), 256-264.

[18] Wahr, J. A., Gerber, M., Venitz, J., & Baliga, N. (2001). Allosteric modification of oxygen delivery by hemoglobin. *Anesthesia & Analgesia*, *92*(3), 615-620.

[19] Wouters, B. G., Delahoussaye, Y. M., Evans, J. W., Birrell, G. W., Dorie, M. J., Wang, J., ... & Brown, J. M. (2001). Mitochondrial dysfunction after aerobic exposure to the hypoxic cytotoxin tirapazamine. *Cancer research*, *61*(1), 145-152.

[20] Coleman, C. N., Bump, E. A., & Kramer, R. A. (1988). Chemical modifiers of cancer treatment. *Journal of Clinical Oncology*, *6*(4), 709-733.

[21] Zeman, E. M., Brown, J. M., Lemmon, M. J., Hirst, V. K., & Lee, W. W. (1986). SR-4233: a new bioreductive agent with high selective toxicity for hypoxic mammalian cells. *International Journal of Radiation Oncology* Biology* Physics*, *12*(7), 1239-1242.

[22] Rickard, A. G., Palmer, G. M., & Dewhirst, M. W. (2019). Clinical and pre-clinical methods for quantifying tumor hypoxia. In Hypoxia and Cancer Metastasis (pp. 19-41). Springer, Cham.

[23] Teicher, B. A., Herman, T. S., & Menon, K. (1992). Enhancement of fractionated radiation therapy by an experimental concentrated perflubron emulsion (Oxygent®) in the Lewis lung carcinoma. *Biomaterials, Artificial Cells and Immobilization Biotechnology*, *20*(2-4), 899-902.

[24] Kavanagh, B. D., Coffey, B. E., Needham, D., Hochmuth, R. M., & Dewhirst, M. W. (1993). The effect of flunarizine on erythrocyte suspension viscosity under conditions of extreme hypoxia, low pH, and lactate treatment. *British journal of cancer*, *67*(4), 734.

[25] Moeller, B. J., Richardson, R. A., & Dewhirst, M. W. (2007). Hypoxia and radiotherapy: opportunities for improved outcomes in cancer treatment. Cancer and Metastasis Reviews, 26(2), 241-248.

[26] Silva, P., Homer, J. J., Slevin, N. J., Musgrove, B. T., Sloan, P., Price, P., & West, C. M. (2007). Clinical and biological factors affecting response to radiotherapy in patients with head and neck cancer: a review. Clinical Otolaryngology, 32(5), 337-345

[27] Sun, H. C., Qiu, Z. J., Liu, J., Sun, J., Jiang, T., Huang, K. J., ... & Huang, C. (2007). Expression of hypoxia-inducible factor-1 alpha and associated proteins in pancreatic ductal adenocarcinoma and their impact on prognosis. International journal of oncology, 30(6), 1359-1367

[28] Moeller, B. J., Dreher, M. R., Rabbani, Z. N., Schroeder, T., Cao, Y., Li, C. Y., & Dewhirst, M. W. (2005). Pleiotropic effects of HIF-1 blockade on tumor radiosensitivity. Cancer cell, 8(2), 99-110.

[29] Kim, K. J., Li, B., Winer, J., Armanini, M., Gillett, N., Phillips, H. S., & Ferrara, N. (1993). Inhibition of vascular endothelial growth factor-induced angiogenesis suppresses tumour growth in vivo. Nature, 362(6423), 841-844.

[30] Shrieve, D. C., & Harris, J. W. (1985). The in vitro sensitivity of chronically hypoxic EMT6/SF cells to X-radiation and hypoxic cell radiosensitizers. International Journal of Radiation Biology and Related Studies in Physics, Chemistry and Medicine, 48(1), 127-138.

[31] Xu, M., Wang, P., Sun, S., Gao, L., Sun, L., Zhang, L., ... & Liang, X. (2020). Smart strategies to overcome tumor hypoxia toward the enhancement of cancer therapy. Nanoscale, 12(42), 21519-21533.

[32] Song, G., Liang, C., Gong, H., Li, M., Zheng, X., Cheng, L., ... & Liu, Z. (2015). Core–shell MnSe@ Bi2Se3 fabricated via a cation exchange method as novel

nanotheranostics for multimodal imaging and synergistic thermoradiotherapy. Advanced materials, 27(40), 6110-6117.

[33] Hu, D., Sheng, Z., Gao, G., Siu, F., Liu, C., Wan, Q., ... & Cai, L. (2016). Activatable albumin-photosensitizer nanoassemblies for triple-modal imaging and thermal-modulated photodynamic therapy of cancer. Biomaterials, 93, 10-19.

[34] Lyu, M., Zhu, D., Duo, Y., Li, Y., & Quan, H. (2020). Bimetallic nanodots for tri-modal CT/MRI/PA imaging and hypoxia-resistant thermoradiotherapy in the NIR-II biological windows. Biomaterials, 233, 119656.

[35] Gong, H., Chao, Y., Xiang, J., Han, X., Song, G., Feng, L., ... & Liu, Z. (2016). Hyaluronidase to enhance nanoparticle-based photodynamic tumor therapy. Nano letters, 16(4), 2512-2521.

[36] Sorg, B. S., Hardee, M. E., Agarwal, N., Moeller, B. J., & Dewhirst, M. W. (2008). Spectral imaging facilitates visualization and measurements of unstable and abnormal microvascular oxygen transport in tumors. Journal of biomedical optics, 13(1), 014026.

[37] Thomlinson, R. H., & Gray, L. H. (1955). The histological structure of some human lung cancers and the possible implications for radiotherapy. British journal of cancer, 9(4), 539.

[38] Secomb, T. W., Hsu, R., Park, E. Y., & Dewhirst, M. W. (2004). Green's function methods for analysis of oxygen delivery to tissue by microvascular networks. Annals of biomedical engineering, 32(11), 1519-1529.

[39] Dewhirst, M. W., Kimura, H., Rehmus, S. W., Braun, R. D., Papahadjopoulos, D., Hong, K., & Secomb, T. W. (1996). Microvascular studies on the origins of perfusion-limited hypoxia. The British journal of cancer. Supplement, 27, S247.ery

[40] Eddy, H. A., & Casarett, G. W. (1973). Development of the vascular system in the hamster malignant neurilemmoma. Microvascular Research, 6(1), 63-82.

[41] Chaplin, D. J., Durand, R. E., & Olive, P. L. (1986). Acute hypoxia in tumors: implications for modifiers of radiation effects. International Journal of Radiation Oncology* Biology* Physics, 12(8), 1279-1282

[42] Dewhirst, M. W. (2009). Relationships between cycling hypoxia, HIF-1, angiogenesis and oxidative stress. Radiation research, 172(6), 653-665.

[43] Cosse, J. P., & Michiels, C. (2008). Tumour hypoxia affects the responsiveness of cancer cells to chemotherapy and promotes cancer progression. Anti-Cancer Agents in Medicinal Chemistry (Formerly Current Medicinal Chemistry-Anti-Cancer Agents), 8(7), 790-797.

[44] Vaupel, P., & Mayer, A. (2007). Hypoxia in cancer: significance and impact on clinical outcome. Cancer and Metastasis Reviews, 26(2), 225-239.

[45] Sullivan, R., & Graham, C. H. (2007). Hypoxia-driven selection of the metastatic phenotype. Cancer and Metastasis Reviews, 26(2), 319-331.

[46] Merck, G. (1848). Vorläufige Notiz über eine neue organische Base im Opium. Justus Liebigs Annalen der Chemie, 66(1), 125-128.

[47] Liu, H. M., & Tu, Y. K. (2002). The efficacy of papaverine administration by different routes for the treatment of experimental acute cerebral vasospasm. Journal of clinical neuroscience, 9(5), 561-565.

[48] Chappie, T. A., Humphrey, J. M., Allen, M. P., Estep, K. G., Fox, C. B., Lebel, L. A., ... & Yang, F. V. (2007). Discovery of a series of 6, 7-dimethoxy-4-pyrrolidylquinazoline PDE10A inhibitors. Journal of medicinal chemistry, 50(2), 182-185.

[49] Goto, T., Matsushima, H., Kasuya, Y., Hosaka, Y., Kitamura, T., Kawabe, K., ... & Takeda, K. (1999). The effect of papaverine on morphologic differentiation, proliferation and invasive potential of human prostatic cancer LNCaP cells. International journal of urology, 6(6), 314-319.

[50] Huang, H., Li, L. J., Zhang, H. B., & Wei, A. Y. (2017). Papaverine selectively inhibits human prostate cancer cell (PC-3) growth by inducing mitochondrial mediated apoptosis, cell cycle arrest and downregulation of NF-κB/PI3K/Akt signalling pathway. J. BUON, 22(1), 112-118.

[51] Afzali, M., Ghaeli, P., Khanavi, M., Parsa, M., Montazeri, H., Ghahremani, M. H., & Ostad, S. N. (2015). Non-addictive opium alkaloids selectively induce apoptosis in cancer cells compared to normal cells. DARU Journal of Pharmaceutical Sciences, 23(1), 16.

[52] Sajadian, S., Vatankhah, M., Majdzadeh, M., Kouhsari, S. M., Ghahremani, M. H., & Ostad, S. N. (2015). Cell cycle arrest and apoptogenic properties of opium alkaloids noscapine and papaverine on breast cancer stem cells. Toxicology mechanisms and methods, 25(5), 388-395.

[53] Noureini, S. K., & Wink, M. (2014). Antiproliferative effect of the isoquinoline alkaloid papaverine in hepatocarcinoma HepG-2 cells—Inhibition of telomerase and induction of senescence. Molecules, 19(8), 11846-11859.

[54] Fix, S. M., Papadopoulou, V., Velds, H., Kasoji, S. K., Rivera, J. N., Borden, M. A., ... & Dayton, P. A. (2018). Oxygen microbubbles improve radiotherapy tumor control in a rat fibrosarcoma model–A preliminary study. PLoS One, 13(4), e0195667.

[55] Evans, W. C. (2009). Trease and evans' pharmacognosy E-book. Elsevier Health Sciences.

[56] Helson, L., Konbun, L., & Young, C. W. (1974). Papaverine-induced changes in cultured human melanoma cells. Biochemical Pharmacology, 23(20), 2917-2920.

[57] Benej, M., Hong, X., Vibhute, S., Scott, S., Wu, J., Graves, E., ... & Denko, N. C. (2018). Papaverine and its derivatives radiosensitize solid tumors by inhibiting mitochondrial metabolism. Proceedings of the National Academy of Sciences, 115(42), 10756-10761.

[58] Siuciak, J. A., Chapin, D. S., Harms, J. F., Lebel, L. A., McCarthy, S. A., Chambers, L., ... & Schmidt, C. J. (2006). Inhibition of the striatum-enriched phosphodiesterase PDE10A: a novel approach to the treatment of psychosis. Neuropharmacology, 51(2), 386-396.

[59] Secomb, T. W., R. Hsu, N. B. Beamer, and B. M. Coull. Theoretical simulation of oxygen transport to brain by networks of microvessels: Effects of oxygen supply and demand on tissue hypoxia. Microcirculation 7:237–247, 2000.

[60] Intaglietta, M., Silverman, N. R., & Tompkins, W. R. (1975). Capillary flow velocity measurements in vivo and in situ by television methods. Microvascular research, 10(2), 165-179.

[61] Secomb, T. W., Hsu, R., Ong, E. T., Gross, J. F., & Dewhirst, M. W. (1995). Analysis of the effects of oxygen supply and demand on hypoxic fraction in tumors. Acta Oncologica, 34(3), 313-316.

[62] Secomb, T. W., Hsu, R., Dewhirst, M. W., Klitzman, B., & Gross, J. F. (1993). Analysis of oxygen transport to tumor tissue by microvascular networks. International Journal of Radiation Oncology* Biology* Physics, 25(3), 481-489.

[63] Hsu, R., & Secomb, T. W. (1989). A Green's function method for analysis of oxygen delivery to tissue by microvascular networks. *Mathematical biosciences*, *96*(1), 61-78.

[64] Secomb, T. W., R. Hsu, R. D. Braun, J. R. Ross, J. F. Gross, and M. W. Dewhirst. Theoretical simulation of oxygen transport to tumors by three-dimensional networks of microvessels. Adv. Exp. Med. Biol. 454:629–634, 1998.

[65] Sørensen, B. S., & Horsman, M. R. (2020). Tumor hypoxia: impact on radiation therapy and molecular pathways. Frontiers in oncology, 10, 562.

[66] Kaanders, J. H., Bussink, J., & van der Kogel, A. J. (2004, July). Clinical studies of hypoxia modification in radiotherapy. In Seminars in radiation oncology (Vol. 14, No. 3, pp. 233-240). WB Saunders.

[67] Ritschel, W. A., & Hammer, G. V. (1977). Pharmacokinetics of papaverine in man. International journal of clinical pharmacology and biopharmacy, 15(5), 227-228.

[68] Bardelmeijer, H. A., Buckle, T., Ouwehand, M., Beijnen, J. H., Schellens, J. H. M., & Van Tellingen, O. (2003). Cannulation of the jugular vein in mice: a method for serial withdrawal of blood samples. *Laboratory animals*, *37*(3), 181-187.

[69] Redler, G., Epel, B., & Halpern, H. J. (2014). What we learn from in vivo EPR oxygen images. In Oxygen Transport to Tissue XXXVI (pp. 121-126). Springer, New York, NY.